

Li X-F, Fowler HJ, Forsythe N, Blenkinsop S, Pritchard D.

[The Karakoram/Western Tibetan Vortex: seasonal and year-to-year variability.](#)

Climate Dynamics 2018

DOI: <https://doi.org/10.1007/s00382-018-4118-2>

Copyright:

© The Authors 2018. This article is an open access publication

DOI link to article:

<https://doi.org/10.1007/s00382-018-4118-2>

Date deposited:

23/02/2018



This work is licensed under a [Creative Commons Attribution 4.0 International License](https://creativecommons.org/licenses/by/4.0/)



The Karakoram/Western Tibetan vortex: seasonal and year-to-year variability

Xiao-Feng Li¹ · Hayley J. Fowler¹ · Nathan Forsythe¹ · Stephen Blenkinsop¹ · David Pritchard¹

Received: 22 August 2017 / Accepted: 2 February 2018
© The Author(s) 2018. This article is an open access publication

Abstract

The “Karakoram Vortex” (KV), hereafter also referred to as the “Western Tibetan Vortex” (WTV), has recently been recognized as a large-scale atmospheric circulation system related to warmer (cooler) near-surface and mid-lower troposphere temperatures above the Karakoram in the western Tibetan Plateau (TP). It is characterized by a deep, anti-cyclonic (cyclonic) wind anomaly associated with higher (lower) geopotential height in the troposphere, during winter and summer seasons. In this study, we further investigate the seasonality and basic features of the WTV in all four seasons, and explore its year-to-year variability and influence on regional climate. We find the WTV accounts for the majority of year-to-year circulation variability over the WTP as it can explain over 50% ($R^2 \geq 0.5$) variance of the WTP circulation on multiple levels throughout the troposphere, which declines towards the eastern side of the TP in most seasons. The WTV is not only more (less) active but also has a bigger (smaller) domain area, with a deeper (shallower) structure, in winter and spring (summer and autumn). We find that the WTV is sensitive to both the location and intensity of the Subtropical Westerly Jet (SWJ), but the relationship is highly dependent on the climatological mean location of SWJ axes relative to the TP in different seasons. We also show that the WTV significantly modulates surface and stratospheric air temperatures, north–south precipitation patterns and total column ozone surrounding the western TP. As such, the WTV has important implications for the understanding of atmospheric, hydrological and glaciological variability over the TP.

Keywords Karakoram vortex · Western Tibetan vortex · Subtropical westerly jet · Precipitation · Ozone · Temperature · Tibetan plateau

1 Introduction

The rugged terrain and low population density over the Western Tibetan Plateau (WTP) results in its very sparse weather station coverage. Practically, this has led to less understanding of climatic and atmospheric variability over this region than over the neighbouring Eastern Tibetan Plateau (ETP) (e.g., Wu et al. 2015). However, recent progress on understanding the main drivers of atmospheric variability has identified a deep vortex system over the WTP—the Karakoram Vortex (KV) (Forsythe et al. 2017). Due to its broader influence over the WTP, the central TP and surrounding areas, we here use the term “Western Tibetan Vortex” (WTV) to describe the KV. Forsythe et al. (2017)

report that the WTV is responsible for a large portion of air temperature variability at the near surface and in the mid-lower troposphere over the WTP, centered on the Karakoram. They suggest that this variability provides a mechanism with which to understand variability in glacier melt and river flows over the WTP and sheds new light on the “Karakoram anomaly”—the recent anomalous expansion or stability of glaciers in the Karakoram region, compared to the rapid deglaciation of glaciers further east in the Himalaya (e.g., Hewitt 2005; Bolch et al. 2012; Kääb et al. 2012; Gardelle et al. 2012; Jacob et al. 2012; Pratap et al. 2016; Zhou et al. 2017).

Forsythe et al. (2017) show that: (1) horizontally, the WTV exhibits as an anti-cyclonic (cyclonic) wind anomaly associated with higher (lower) geopotential height (HGT) and warmer (cooler) temperatures in the mid-lower troposphere over the WTP; (2) vertically, the core mass column of the WTV extends from the near surface of the WTP (~500 hPa) to above the tropopause; (3) the connection of

✉ Xiao-Feng Li
Xiaofeng.Li@newcastle.ac.uk

¹ School of Engineering, Newcastle University,
Newcastle upon Tyne NE1 7RU, UK

air temperature in the mid-lower troposphere and the WTV is mainly through an adiabatic rising/sinking process; (4) the summertime WTV is partly coupled with the South Asia summer monsoon (SASM), as the southern flank of the WTV overlaps the prevailing area of the SASM; (5) WTV variability explains a large proportion of near surface air temperature variability over the WTP centered on the Karakoram, both in late winter (JFM) and summer (JJA); (6) the WTV exists year round. Thus, Forsythe et al. (2017) show that the WTV is an important atmospheric vortex system driving atmospheric variability over the WTP.

The seasonal signature of the WTV has also been noted in previous studies. Watanabe and Yamazaki (2012) found that the anticyclonic anomaly in the Subtropical Westerly Jet (SWJ) over the Western Tibetan Plateau influences the intra-seasonal variability of monsoon rain over South Asia, Southeast Asia, and probably also over East Asia in early summer. Zhao et al. (2014) noted similar anticyclonic/cyclonic anomalies over the WTP, which play a role in transporting water vapour from the subtropical Indian Ocean to the Tarim Basin, and have resulted in recent changes in precipitation over the Tarim Basin during the summer season. These studies imply that WTV variability could also be important for understanding climatic variability over the plain and basin areas surrounding the Tibetan Plateau.

Although the WTV was identified by Forsythe et al. (2017) and has been demonstrated to significantly modulate the near surface air temperature variability over the Karakoram in late winter (JFM) and summer (JJA), there are still gaps in our understanding of its basic features and seasonality. Similarly, the influence of the WTV on the year-to-year variability of climate in the wider region has not been fully investigated. In this study, we further investigate the seasonality and basic features of the WTV in all four seasons, and explore its year-to-year variability and influence on the surrounding climate, so extending the research of Forsythe et al. (2017).

The remainder of this paper is organized as follows. Section 2 presents data and methods. In this section, we develop a monthly Karakoram Zonal Index (KZI), according to the seasonal KZI defined by Forsythe et al. (2017). The monthly KZI can express the variability of the WTV year-round, whilst its seasonal mean is identical to the seasonal KZI of Forsythe et al. (2017). In Sect. 3, we examine seasonal variations in the horizontal and vertical structure of the WTV in wind, HGT and air temperature fields, and the adiabatic processes associated with WTV variability. In Sect. 4, we present the seasonal variation of the intensity of the WTV, as well as the seasonal change in the dominant area of the WTV (defined as the area with significant correlations between the KZI and HGT over the TP). Then, the connections between year-to-year variability of the WTV and the SWJ are investigated in Sect. 5. In Sect. 6, we examine the

varying structures associated with the WTV in year-to-year variability. Finally, a discussion of the results and our conclusions are presented in Sect. 7.

2 Data and methods

As the WTV is a local circulation system located over the Western Tibetan Plateau, we employ both monthly and daily ERA-Interim reanalysis datasets (Dee et al. 2011) in this analysis (<http://apps.ecmwf.int/datasets/>) due to their high spatial resolution: $0.75^\circ \times 0.75^\circ$ in the horizontal direction and 26 levels in the vertical direction. The variables used from ERA-Interim include the zonal wind velocity (m s^{-1}), the meridional wind velocity (m s^{-1}), the vertical wind velocity (Pa s^{-1}), the geopotential height (HGT, $\text{m}^2 \text{s}^{-2}$ or gpm) and the air temperature (K) on multiple isobaric levels, the surface air temperature (K) at 2 m elevation, and the total column ozone (10^{-2} g m^{-2}). The precipitation (mm day^{-1}) is from the Asian precipitation-highly-resolved observational data integration towards evaluation (APHRODITE) dataset (Yatagai et al. 2012) which includes dense station observations over the high mountain area and is at a spatial resolution of $0.25^\circ \times 0.25^\circ$. We focus on the 1979–2016 period, except for the study of precipitation as the APHRODITE dataset only covers the period 1979–2007. We define the circulation anomaly as the departure from the climatological mean circulation during the reference period, 1979–2010; but the precipitation anomaly is calculated based on the climatological mean of 1979–2007 due to the shorter time-period of precipitation data. In calculating the monthly anomaly time series, the climatological mean is defined as the monthly annual cycle. For daily anomalies, the climatological mean is defined as the first four harmonics of the daily annual cycle.

To examine the connection between the WTV and other variables, we use both the Pearson correlation coefficient and the slope of linear regression. The Pearson correlation coefficient (R) and the slope of linear regression in a season (winter, spring, summer or autumn) or in the annual mean are calculated based on the seasonal mean or annual mean time series of two climate modes (for example, the WTV intensity and surface air temperature) during 1979–2016 (or 1979–2007 for the precipitation data). More details can be found in Li et al. (2013). The explained variance is calculated as the square of the Pearson correlation coefficient, i.e. the R^2 . As the linear trend and the low frequency variability for the period of 1979–2016 (or 1979–2007 for the precipitation data) was not removed for each season before the calculations, the results in this study represent both the inter-annual and longer-term variability, which we hereafter refer to as the year-to-year variability. Following Zar (1984) and Li et al. (2013), the efficient number of degrees of freedom are taken into account in the 2-tailed student-t test of the correlations and linear regressions.

Following Forsythe et al. (2017), the “Karakoram Zonal Shear” (KZS) is used to depict the general zonal wind difference between the north and south branch of the WTV. The KZS is defined as follows:

$$KZS = \overline{U_N} - \overline{U_S} \quad (1)$$

where “ $\overline{}$ ” denotes the area mean. U_N and U_S are the zonal wind anomalies over the north (40°N–50°N, 52.5°E–86.25°E) and south (20°N–32.5°N, 52.5°E–93.75°E) branches of the WTV, respectively. In this study, the KZS is calculated at both the 200 and 500 hPa. From Fig. 1, we can see the location and scope of the north and south branches of the WTV relative to the subtropical westerly jet at the 200 hPa level. It should be noted that both the north and south branches of the WTV are located within the domain of the subtropical westerlies, except for summer when the tropical easterly trade wind moves north into the south branch of the WTV. This coincides with the movement of the tropical easterly trade wind belt and the subtropical westerly jet (SWJ) to their northernmost locations in summer, with the SWJ axis located on the north side of the Tibetan Plateau.

After the removal of the annual cycle from the KZS and then standardizing it, we derive the Karakoram Zonal Index (KZI) (as Forsythe et al. 2017). Specifically, we expanded the KZI from the seasonal index of Forsythe et al. (2017) to a monthly index to try to depict in more detail the continuous intensity variations of the WTV over the annual cycle. The continuous monthly KZI is therefore defined at 200 hPa for consistency with the seasonal KZI defined in our previous study (Forsythe et al. 2017) as follows:

$$KZI = \tilde{KZSA}, \quad (2)$$

where KZS anomaly (KZSA) is at 200 hPa, which is defined as follows:

$$KZSA = \overline{U'_N} - \overline{U'_S}, \quad (3)$$

where “ $\overline{}$ ” denotes the monthly anomaly, a departure from the annual cycle defined on the 1979–2010 base period (consistent with the base period used in Forsythe et al. 2017). So, the signal of the annual cycle of zonal wind due to seasonal changes of the solar angle is removed (or suppressed) in the KZSA. \tilde{KZSA} is the normalization of KZSA for a given year n and month m and calculated as follows:

$$\tilde{KZSA}_{m,n} = \frac{KZSA^*_{m,n}}{S}, \quad (4)$$

where $KZSA^*_{m,n}$ is the monthly anomaly of $KZSA_{m,n}$, a departure from the mean $KZSA_{m,n}$ over the 1979–2010 base period,

$$KZSA^*_{m,n} = KZSA_{m,n} - \frac{1}{12 \times 32} \sum_{n=1979}^{2010} \sum_{m=1}^{12} KZSA_{m,n}, \quad (5)$$

and S is the standard deviation of the monthly anomaly $KZSA^*_{m,n}$ time series over the base period, i.e.,

$$S = \sqrt{\frac{1}{12 \times 32} \sum_{n=1979}^{2010} \sum_{m=1}^{12} KZSA^*_{m,n}^2}. \quad (6)$$

The KZI then represents the standardized north–south gradient of the anomalous zonal winds around the Karakoram from month to month, as shown in Fig. 2. In its seasonal mean, the KZI is identical to the index defined by Forsythe et al. (2017).

3 The western Tibetan vortex in wind, HGT and air temperature fields

To study the basic features of the WTV, we investigate the horizontal structure, vertical structure, and the related adiabatic processes of the WTV in all four seasons and in the annual mean data. Through these analyses, we can see the WTV prevails and is substantial over the WTV all year around, although there are minor seasonal differences. Besides, we can see that the WTV not only has a deep structure, but also has a large horizontal spatial scale that is comparable to the South Asian summer monsoon or the Indian summer monsoon, implying it is a large-scale circulation system important for the WTP and neighbouring areas.

3.1 Horizontal structure

Although there are obvious seasonal differences, the WTV structure is a common feature of atmospheric circulation over the WTP in all four seasons (Fig. 3a–d). The spatial pattern of correlations between the KZI and both horizontal wind and geopotential height (HGT) at 500 hPa (the near surface of the Tibetan Plateau) reveal both anti-cyclonic (cyclonic) wind structures and positive (negative) HGT anomalies during a positive (negative) KZI phase. In all seasons, these atmospheric structures (correlation patterns) are centred over the WTP (Fig. 3a–d); or, more precisely, just to the southwest of the Karakoram. This anti-cyclonic vortex structure over the WTP is associated with warmer air temperatures in the mid-troposphere (Fig. 4a–d), which is identical to the Karakoram Vortex reported by Forsythe et al. (2017) for late winter (JFM) and summer (JJA). The similar vortex structure in the horizontal wind and HGT fields is also detected at higher levels (not shown), suggesting the WTV has a deep structure with quasi-barotropic features (also see the following section b—vertical structure) all year round. Therefore, the WTV prevails in all four seasons over the WTP.

Climatological Winds

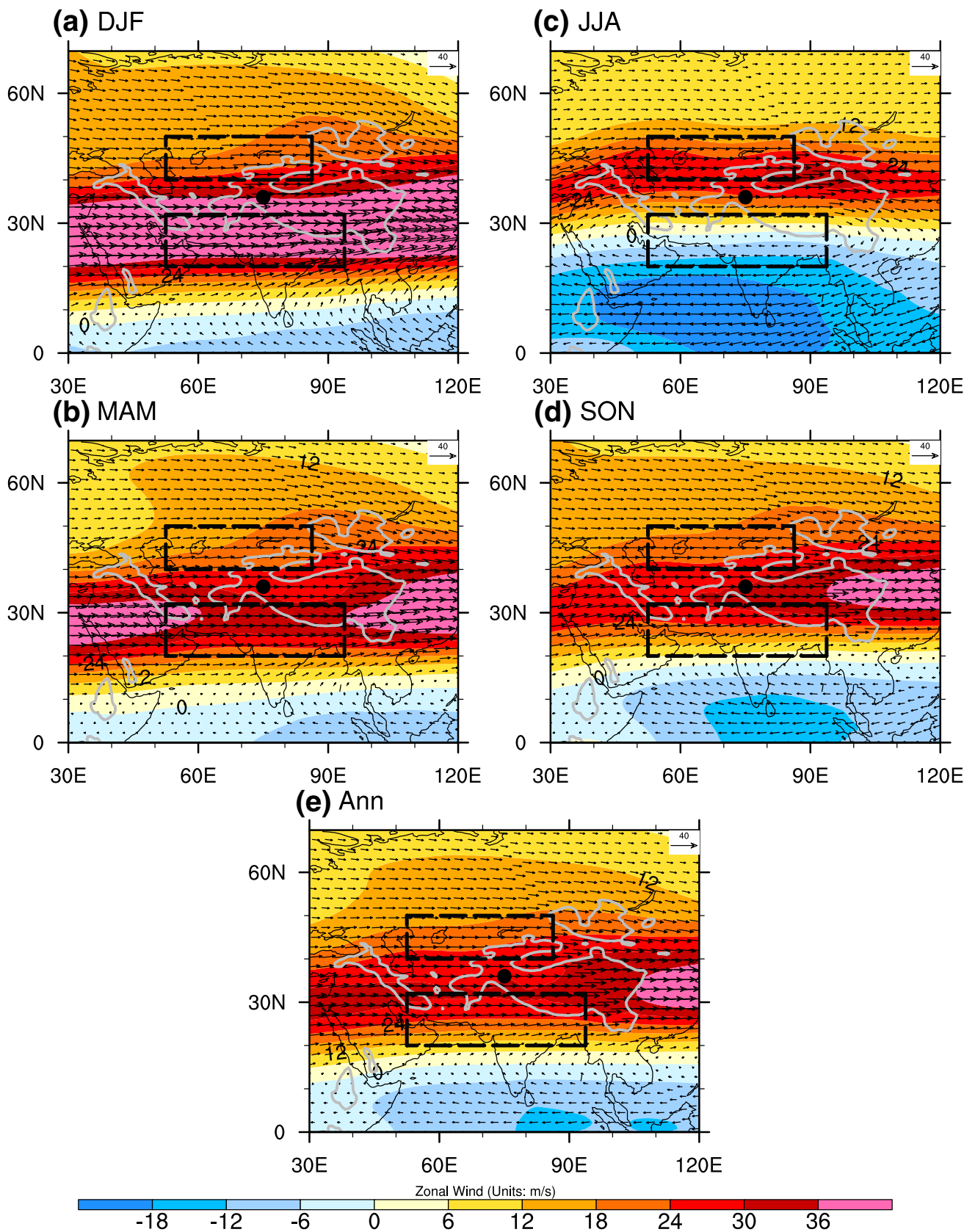


Fig. 1 Climatological mean horizontal wind vectors (m/s) and zonal wind speed (colour-shaded, m/s) at the 200-hPa level over the TP for **a** winter (DJF), **b** spring (MAM), **c** summer (JJA), **d** autumn (SON) and **e** annual mean for 1979–2016. The wind vector length scale is shown in the upper right corner of panels; the bold curved grey lines denote topography above 1500 m. The black point denotes the central position (36°N, 75°E) of the Karakoram focus area. The bold dash rectangles denote the north (40°N–50°N, 52.5°E–86.25°E) and south (20°N–32.5°N, 52.5°E–93.75°E) branches of the WTV

On average, the WTV is centred on the southwest tail of the Tibetan Plateau with its area of influence extending to the wider region (from ~50°E to ~90°E and 25°N to ~40°N over the WTP). It shows relatively weak signals over the ETP east of 90°E, as evidenced by the correlations of annual mean values (Figs. 3e, 4e). The features of the WTV show slight seasonal variations. The WTV has its largest area of influence in winter (Figs. 3a, 4a), as significant correlations in HGT and temperature fields extend from ~40°E to east of 90°E, covering the whole of the Tibetan Plateau. In spring, its domain shrinks slightly (Figs. 3b, 4b), and reaches its smallest area in summer when its core contains only the WTP, within 60°E to ~80°E (Figs. 3c, 4c). In autumn, the WTV becomes larger again (Figs. 3d, 4d). Comparing the winter and summer WTV, we can see that the summer WTV is only significantly correlated with the near surface air temperatures at 500 hPa over a small portion of the WTP, while the winter WTV is significantly correlated with near surface air temperatures at 500 hPa over the whole of the Tibetan Plateau, although maximum summer correlations are higher. Another feature we note here from the horizontal wind field is that the WTV exhibits a more circular cyclonic/anti-cyclonic shape in spring and summer than in winter and autumn at the near surface of the WTP.

We emphasize that the spatial extent of the WTV is comparable to that of the south Asian summer monsoon or the Indian summer monsoon system as can be seen from either the horizontal wind, the HGT, or the extent of the significant air temperature correlation with the KZI (Figs. 3, 4). For example, the significant anti-cyclonic wind structures associated with WTV variability in spring (Figs. 3b, 4b) cover the whole Tibetan Plateau and some of the neighbouring plains and basin areas from ~45°E to ~110°E. This suggests that the west-east diameter of this circulation system extends about 6500 km (1° of longitude is around 100 km at the surface in the mid-latitudes)—at least 3–4 times the west-east diameter of Indian Peninsula. Therefore, the WTV is a large-scale circulation system that not only influences the Karakoram area as presented in Forsythe et al. (2017), but also has influence over a wider region including the high mountain TP area outside of the Karakoram and the plain and basin areas neighbouring the TP. The new alias name, “Western Tibetan Vortex”

is therefore intended to clarify and emphasize the large spatial scale of this circulation system.

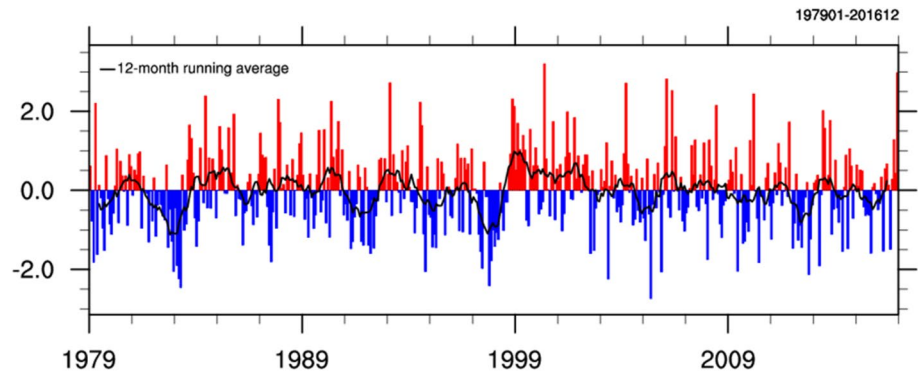
3.2 Vertical structure

The vertical structure of the zonal wind correlations with the WTV (contours in Fig. 5) extends upward from the mid-lower troposphere to the lower stratosphere on both the north and south sides of the WTP, exhibiting as a quasi-barotropic or deep north–south “dipole” feature in all seasons. The deep north–south “dipole” exists in the anomalous zonal wind field, which results from a stronger (weaker) westerly wind in the north of the WTP (from ~35°N to ~55°N) and a weaker (stronger) westerly wind or a stronger (weaker) easterly wind in the south of the WTP (from ~10°N to ~35°N). In winter (Fig. 5a), the response of the zonal wind south of the WTP is much stronger than for the north side, but in other seasons (Fig. 5b–d) the responses of the zonal wind for both sides of the WTP are more comparable. This coincides with stronger wintertime climatological zonal winds to the south of the WTP than to the north of the WTP, as shown in Fig. 1. Further, the core area of zonal wind correlations with the KZI supports the deep north–south “dipole” in the anomalous zonal wind field related to the WTV, as evidenced by the area with absolute correlation coefficients above 0.7, which extend from ~700 to ~100 hPa for both sides of the WTP in the annual mean data (Fig. 5e). This deep north–south “dipole” in the anomalous zonal wind field actually represents a deep KZSA (see “Data and methods”) across multiple levels. So, the anti-cyclonic (cyclonic) WTP corresponds to a deep positive (negative) KZSA throughout the troposphere and the lower stratosphere.

The KZSA is actually only one component of the horizontal rotations of the WTV. Horizontal rotations of the WTV are caused by two components, the anomalous north–south wind shear (i.e. the KZSA) and the anomalous east–west wind shear. To further investigate the vertical profile of the strength of rotations of the WTV in two horizontal dimensions, we employ the horizontal stream function (HSF), as it considers wind shears effects in both horizontal dimensions (Holton 2004). On zonal and meridional dimensions: a positive (negative) HSF denotes anti-cyclonic (cyclonic) circulation. Over the WTP, significant positive correlations (colour shading in Fig. 5) between HSFs and the KZI are observed on multiple levels from ~700 to ~70 hPa in different seasons, overlapping at the central location of the zonal wind “dipole” structure (Fig. 5). This implies that the anti-cyclonic (cyclonic) WTV exists from the mid-lower troposphere to above the tropopause, and again confirms the deep structure of the WTV.

We also note seasonal variations in the rotation features associated with the WTV. The vertical range of the significant rotation anomalies (as denoted by significant

Fig. 2 Monthly time series of the KZI for 1979–2016. The black curve shows the 12-month running average



Horizontal Structure of WTV

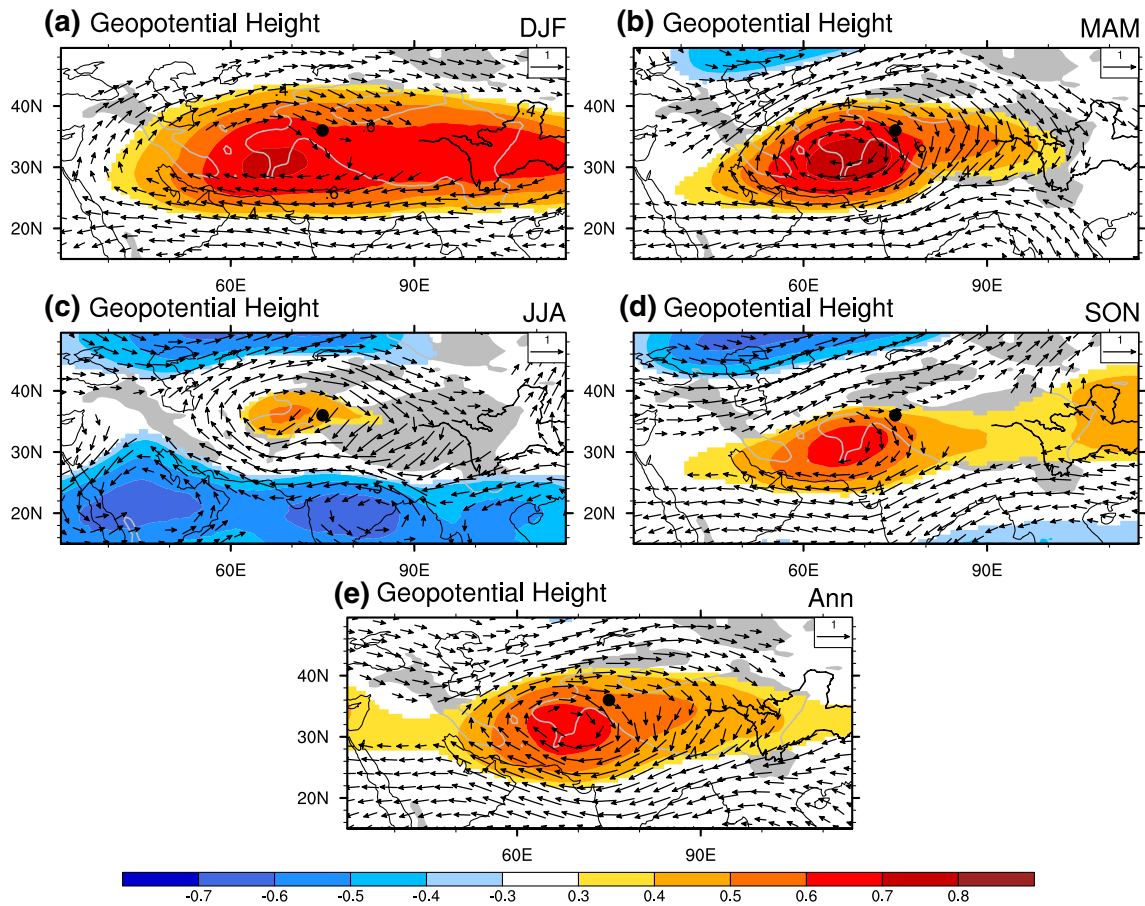


Fig. 3 Correlations between the KZI and geopotential height (HGT) for **a** winter (DJF), **b** spring (MAM), **c** summer (JJA), **d** autumn (SON) and **e** annual mean at the 500 hPa level (the near surface of the Tibetan Plateau) for 1979–2016. Only significant correlations above the 0.05 level are shown, after taking account of the efficient number of degrees of freedom (Zar 1984; Li et al. 2013). Vectors are composites of the correlations with horizontal wind components (U,V): a sig-

nificant vector denotes either one of its components is significant. The correlation length scale is shown in the upper right corner of panels. The black dot denotes the central position (36°N, 75°E) of the Karakoram focus area. The grey shaded area denotes topography above 1500 m. Bold black curves originating in the ETP are respectively the Yangtze River and the Yellow River

correlations) is deeper in winter and spring, as it extends from 700 to 850 hPa up to 70 hPa, while in summer and autumn it extends only from ~600 to 100 hPa. In addition,

rotations in winter are more intense below 500 hPa, whereas for other seasons, the rotations are fairly uniform at different

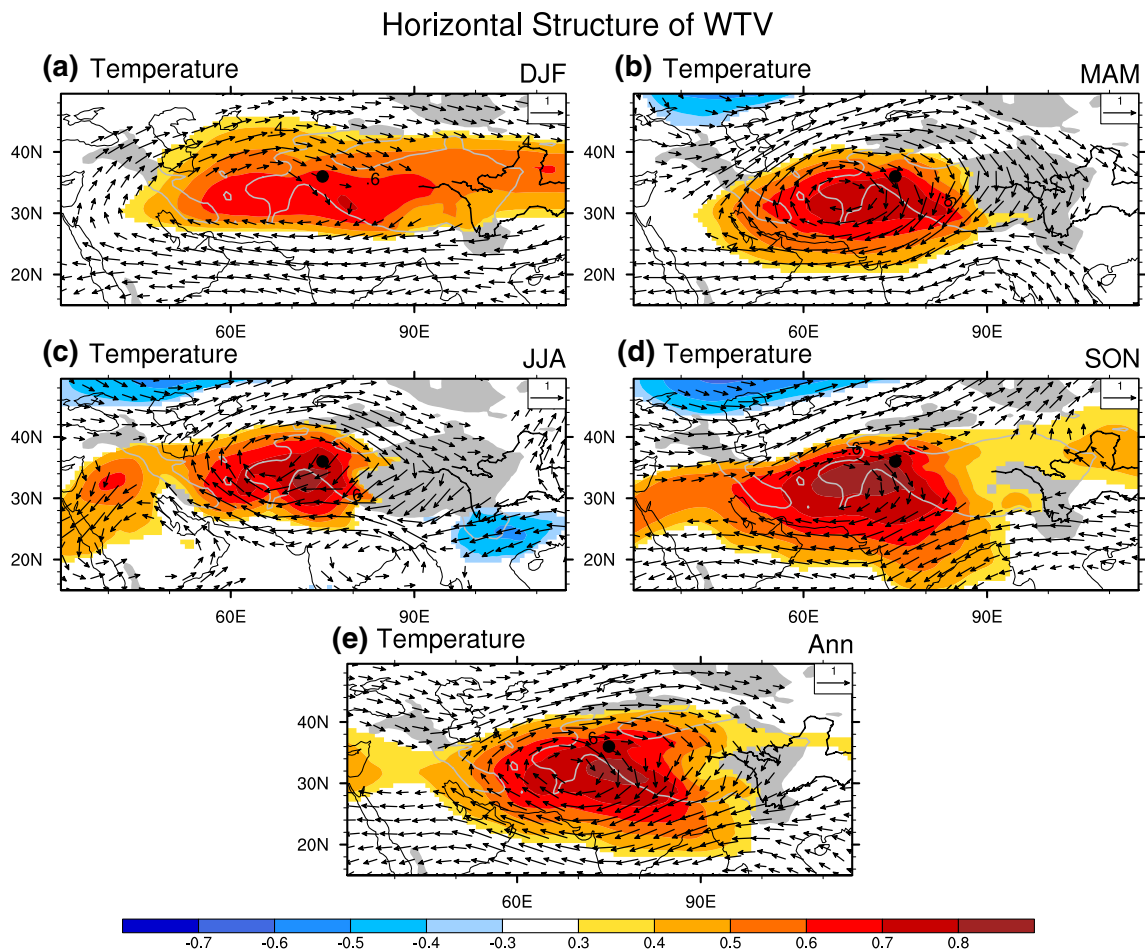


Fig. 4 Correlations between the KZI and air temperature for **a** winter (DJF), **b** spring (MAM), **c** summer (JJA), **d** autumn (SON) and **e** annual mean at the 500 hPa level for 1979–2016. Only significant correlations above the 0.05 level are shown, after taking account of the efficient number of degrees of freedom (Zar 1984; Li et al. 2013). Vectors are composites of the correlations with horizontal wind com-

ponents (U,V): a significant vector denotes either one of its components is significant. The correlation length scale is shown in the upper right corner of panels. The black dot denotes the central position (36°N, 75°E) of the Karakoram focus area. The grey shaded area denotes topography above 1500 m. Bold black curves originating in the ETP are respectively the Yangtze river and the Yellow river

levels. So, the WTV has a deeper structure in winter and spring relative to summer and autumn.

3.3 Adiabatic process

The adiabatic sinking/rising process associated with WTV variability was documented for late winter (JFM) and summer (JJA) in Forsythe et al. (2017). Here, we expand its analysis to all four seasons and the annual mean. Figure 6 shows that positive correlations between HGT (contours) and the KZI are highest above the WTP, overlapping the significant positive correlations of the HSFs with the KZI (colour-shaded in Fig. 5). This suggests that the core of the atmospheric mass column circled by the anomalous rotations associated with the WTV is directly above the

Karakoram: the anti-cyclonic (cyclonic) WTV is responding to more (less) air mass in its core circled by an anomalous anti-cyclonic (cyclonic) wind structure horizontally. Within the core atmospheric mass column of the WTV, significant correlations of the wind vectors with the KZI below 100–150 hPa are exhibited as downward values and are overlapped with the positive correlation between the KZI and air temperature on isobaric surfaces. This suggests that the downward (upward) wind anomaly brings atmospheric mass volume into denser (lighter) pressure levels, causes compression (expansion) of the volume of the atmospheric mass, and results in the increase (decrease) of air temperature: a classic adiabatic process. As a result, the correlation between the KZI and the air temperature in the mid-lower troposphere reaches more

Vertical structure of WTV

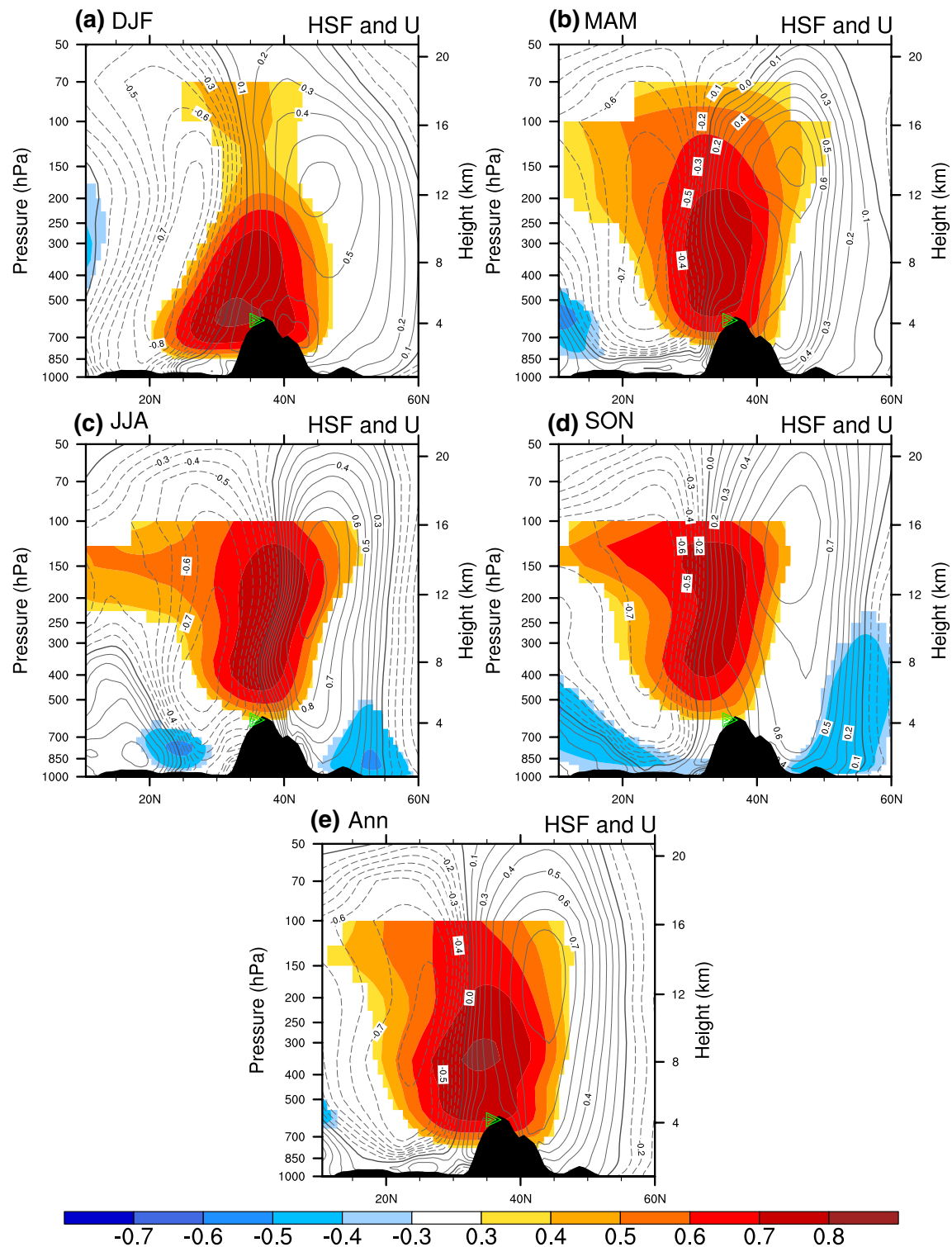


Fig. 5 Correlations between the KZI and zonal wind (U, contour), horizontal stream function (HSF, colour-shading) along a latitudinal profile (across 70°E–80°E) at multiple levels for 1979–2016, **a** winter (DJF), **b** spring (MAM), **c** summer (JJA), **d** autumn (SON) and **e** annual mean. The contour interval is 0.1. The colour-shading **a–e**

only denotes the correlations with HSF significant at the 0.05 level, after taking account of the efficient number of degrees of freedom (Zar 1984; Li et al. 2013). The black shaded area denotes the topography. The green triangle denotes the central Karakoram (36°N, 75°E)

Vertical structure of WTV

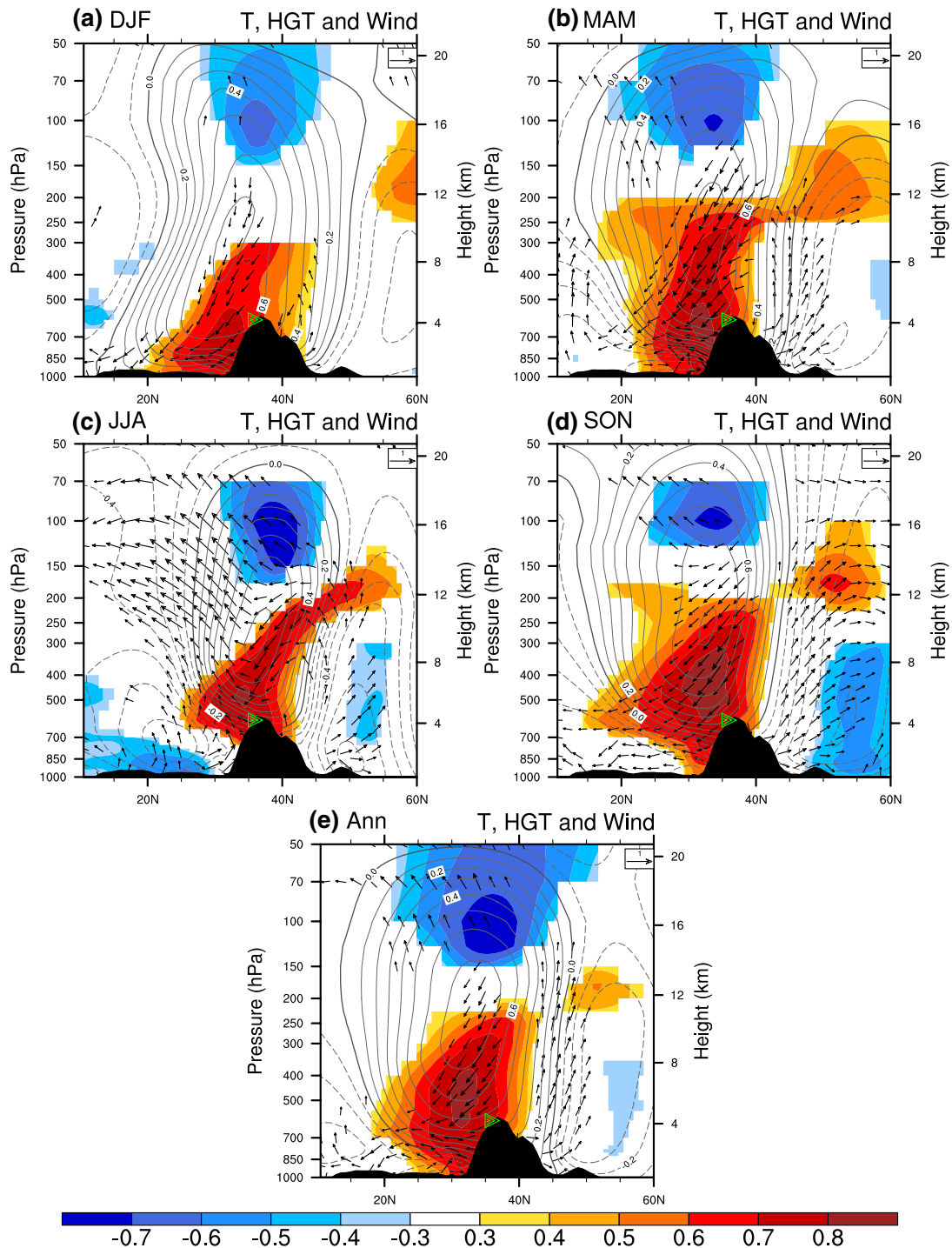


Fig. 6 Correlations between KZI and geopotential height (HGT, contour), air temperature (T, colour-shaded), and vertical wind (arrows) vectors (V,W) along a latitudinal profile (across 70°E–80°E) for 1979–2016. **a** Winter (DJF), **b** spring (MAM), **c** summer (JJA), **d** autumn (SON) and **e** annual mean. The contour interval is 0.1. The colour-shading (**a–e**) denotes the correlations with T significant at the 0.05 level, after taking account of the efficient number of degrees of

freedom (Zar 1984; Li et al. 2013). Vectors are composites of the correlations with meridional and vertical wind components (V,W): a significant vector denotes either one of its components is significant. The correlation length scale is shown in the upper right corner of panels. The black shaded area denotes the topography. The green triangle denotes the central Karakoram (36°N, 75°E)

than 0.7 over large areas of the WTP in most seasons and the annual mean (Figs. 4, 6), suggesting that WTV variability explains a large portion of the WTP's temperature variability through adiabatic processes. We conclude that the adiabatic sinking (rising) process associated with WTV variability is the major mechanism influencing air temperature in the mid-lower troposphere above the WTP in all seasons. This is a verification and extension of the results of Forsythe et al. (2017).

We also find that in winter and spring, air temperature anomalies in the mid-lower troposphere extend downward to the near surface of the plains south of the WTP (at ~ 1000 hPa), while in summer and autumn air temperature anomalies do not extend below 700 hPa, as demonstrated by significant correlations between the KZI and air temperature in Fig. 6. This is consistent with results from the

previous section that show that the WTV has a deeper structure in winter and spring than in summer and autumn.

The air temperature in the lower stratosphere centred at 100 hPa is also significantly negatively correlated with WTV variability in all seasons and for the annual mean (as Forsythe et al. 2017). We also note that the cold anomalies are co-located with anomalous upward wind vectors in all seasons. In particular, the cold anomalies and anomalous upward wind vectors are greatest in summer (Fig. 6). Whether this is also due to adiabatic processes needs further investigation, since the significant vertical motions are not as strong as in the mid-lower troposphere (Fig. 6), but this is out of scope for the current study.

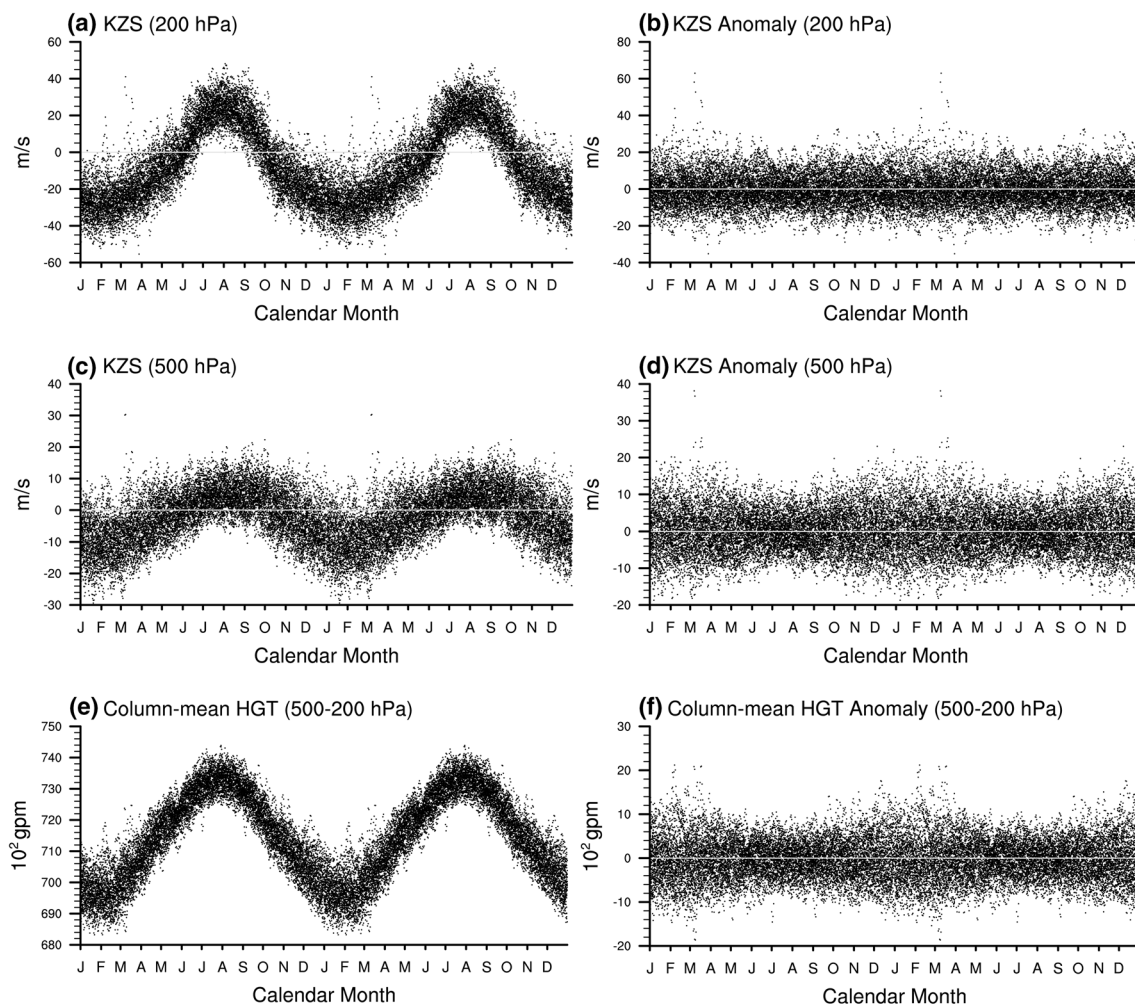


Fig. 7 Daily mean Karakoram zonal shear (KZS) (m/s) and column mean geopotential height (HGT) (metre, gpm) for 1979–2016 as a function of calendar day. **a** KZS at 200 hPa, **c** KZS at 500 hPa, and **e** column mean HGT (gpm) between 200 and 500 hPa within the cen-

tral area (26°N – 45°N , and 60°E – 85°E) of the Karakoram vortex. **b** as **a**, **d** as **c**, and **f** as **e**, but with the climatological mean removed. Annual cycle is repeated to provide continuous information on the cold season

4 Seasonality of KZS intensity and WTV's domain area

4.1 Annual cycle and variance

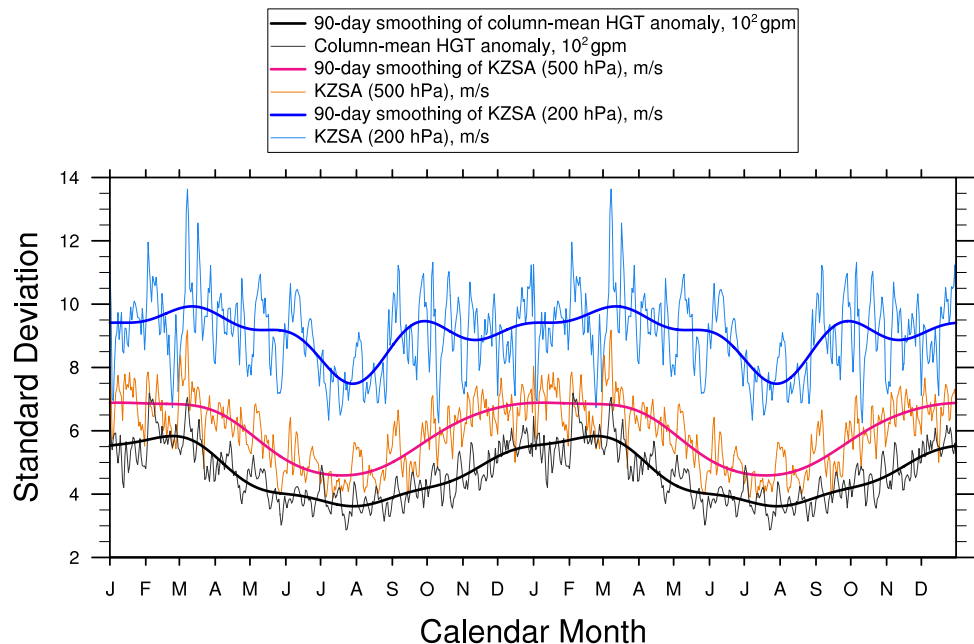
To investigate the seasonally varying climatology of the WTV we use a series of scatterplots of the KZS and the column-mean HGT (Fig. 7) constructed from daily mean data, following the method of Thompson and Wallace (2000). The KZS represents the north–south shift of the zonal wind between the north and south flank of the WTV. The column-mean HGT in the core column of the WTV (500–200 hPa, 26°N–45°N, 60°E–85°E) represents the mass fluctuation in the central location of the WTV. The KZS anomaly and column-mean HGT anomaly are respectively calculated from the zonal wind anomaly and HGT anomaly data from which the annual cycle was removed at each grid point. Time series of all 38 years (1979–2016) are plotted together as a function of calendar date in Fig. 7, which shows the mean annual cycle.

The KZS (Fig. 7a, c) and column-mean HGT (Fig. 7e) above the Karakoram have an obvious seasonal cycle, peaking in summer (JJA) and reaching their lowest values in winter (DJF). As a higher HGT of isobaric surface denotes higher pressure at the same location, this suggests that the pressure over the Karakoram is higher in summer than winter. This coincides with the seasonal movement of the track and intensity changes of the SWJ and the subtropical high (SH) over the Karakoram. The SWJ and SH reach their most northerly (southerly) location during summer (winter) when the westerlies to the

north side of the Karakoram are stronger (weaker) than to the south side, and the pressure over the Karakoram is higher (lower). This results in an anti-cyclonic (cyclonic) KZS and a stronger (weaker) column-mean HGT above the Karakoram in summer (winter).

After the removal of the seasonal cycle, the KZS and column-mean HGT anomalies are shown in Fig. 7b, d, f. In contrast to the seasonal change in intensity of the KZS, i.e. KZS is anti-cyclonic (cyclonic) in summer (winter), the seasonal variance of the KZS anomaly (or KZSA, the normalization of the KZSA is the KZI, see method section) is small (large) in summer (winter). This is evidenced by the KZSA at 200 hPa (Fig. 7b), but more clearly at 500 hPa (Fig. 7d) and column mean HGT of the core region of the WTV (Fig. 7f) in summer (winter) being closer to (further from) zero. This suggests that the absolute magnitude of the WTV can be greater in cold seasons than warm seasons, while the previous section and Forsythe et al. (2017) have both demonstrated that the variability of the WTV, quantified as the KZI, is substantial over the WTP in all seasons. As confirmed in Fig. 8, the standard deviation of the KZSA at 200 hPa (navy and dark blue curves) in June, July and August is much smaller than for other calendar months, while the KZSA at 500 hPa (orange and red curves) and the column-mean HGT anomaly (grey and black curves) show a similar range of variability, suggesting that the WTV has a smaller absolute magnitude of variation in these warm months. Interestingly, the WTV in March (Fig. 8) shows higher standard deviation than for other months, implying that early spring is an important season for WTV variability. Identification of the underlying drivers of these differences in absolute variability

Fig. 8 Standard deviation of daily mean KZS anomaly (KZSA, m/s) at 200 and 500 hPa, column mean HGT anomaly (gpm) between 200 and 500 hPa within the central area (26°N–45°N, and 60°E–85°E), and 90-day running means for 1979–2016 as a function of calendar day. Annual cycle is repeated to provide continuous information for the cold season



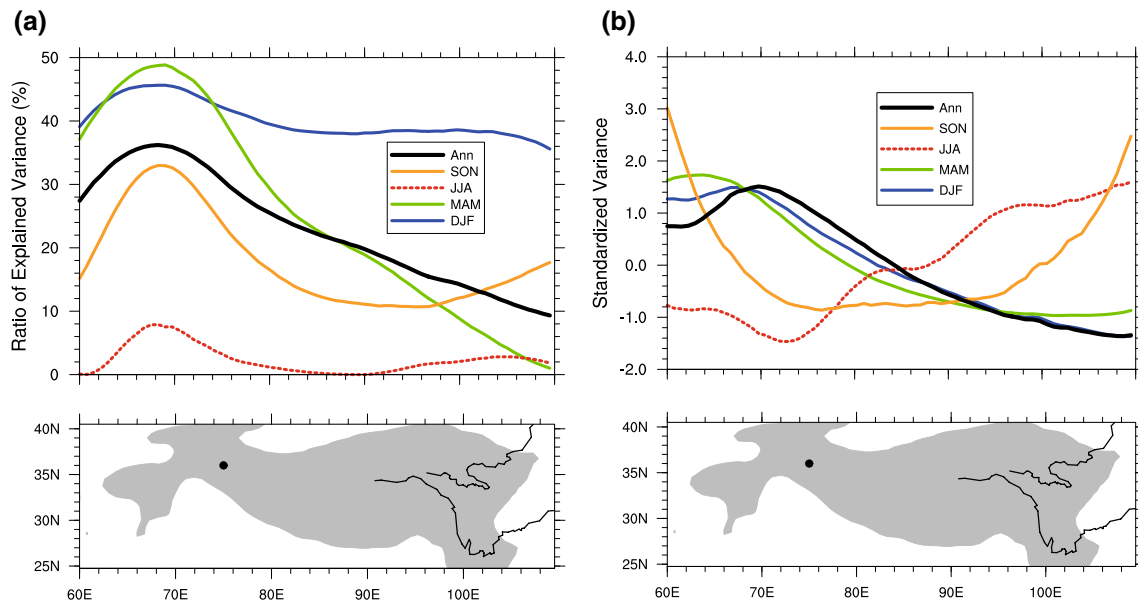


Fig. 9 **a** The ratio (%) of the explained variance of the meridionally-averaged (24.75°N–40.5°N) 500 hPa HGT above the Tibetan Plateau by the standardized WTV intensities as a function of longitude for 1979–2016. **b** is as same as **a**, but for the variance of the meridionally-averaged (24.75°N–40.5°N) 500 hPa HGT above the Tibetan Plateau, which is standardized along the parallel circle between 60°E and 110°E for comparison. Winter (DJF, blue solid line), spring (MAM,

green solid line), summer (JJA, red dashed line), autumn (SON, orange solid line) and annual mean (bold solid line). The topography of Tibetan Plateau is shown in the bottom panel (24.75°N–40.5°N, 60°E–110°E), the grey shaded area denotes the topography above 1500 m. The black dot denotes the central position (36°N, 75°E) of the Karakoram focus area. Bold black curves originating in the ETP are respectively the Yangtze River and the Yellow River

remains a priority for on-going research. We conclude that the WTV has obvious seasonality as its activity becomes weaker in summer and stronger in winter and early spring.

4.2 Seasonal dominance of the WTV over the Tibetan plateau

As shown in Fig. 9a, the WTV's central location is at the western tail of the TP in all seasons, with its dominant area expanding and shrinking seasonally to the surrounding area of the WTP. The central location of the WTV in Fig. 9a is defined as the longitude with the maximum ratio of year-to-year variance of the meridionally-averaged (24.75°N–40.5°N) HGT over the TP explained by WTV variability. This is centred at around 68°E in all seasons and for the annual mean (Fig. 9a). Accompanied by intensity changes of the WTV, the explained variance over the near surface level (500-hPa) of the TP (Fig. 9a) also changes seasonally. In spring and winter, the maximum ratio of explained variance reaches near to 50% and around 45%, respectively; in autumn, the maximum explained variance drops, but is still above 30%; and in summer the maximum explained variance drops to its lowest value, near to 10%. The WTV explains more variance of the meridionally-averaged (24.75°N–40.5°N) 500 hPa HGT over the ETP in winter and explains less variance over the same region

in summer: this suggests that the WTV's dominant area extends further eastward in winter. In addition, the largest contrast between the WTP and the ETP occurs in spring, when explained variance reaches as high as 50% in the WTP, but drops dramatically to near zero eastward on the Tibetan Plateau. This suggests that the WTV is not only more active but its dominant area focuses on the near surface of WTP in spring. Thus, although the central location of the WTV is relatively stable at the western tail of the TP, its dominant area over the near surface of WTP is greater in the winter and smaller in summer, and in spring the WTV's domain is focused more on the WTP.

When comparing the longitudinal-profile of the variance of HGT over the TP (Fig. 9b) with the ratio of explained variance by the WTV (Fig. 9a), we show that the WTV is an important mode of variability for the whole near surface (500-hPa) of the TP. It causes a pattern of “West-Strong, East-Weak”, i.e. the variance of meridionally-averaged (24.75°N–40.5°N) HGT over the WTP is greater than for the ETP, for the annual mean and for most seasons. As shown in Fig. 9b, the pattern of “West-Strong, East-Weak” is observed in the annual mean, spring, and winter. As the WTV explains about half of the variance in HGT over the near surface (500-hPa) of the WTP (Fig. 9a), the results here suggest that WTV variability dominates mid-low tropospheric variability over the TP in the annual mean, spring

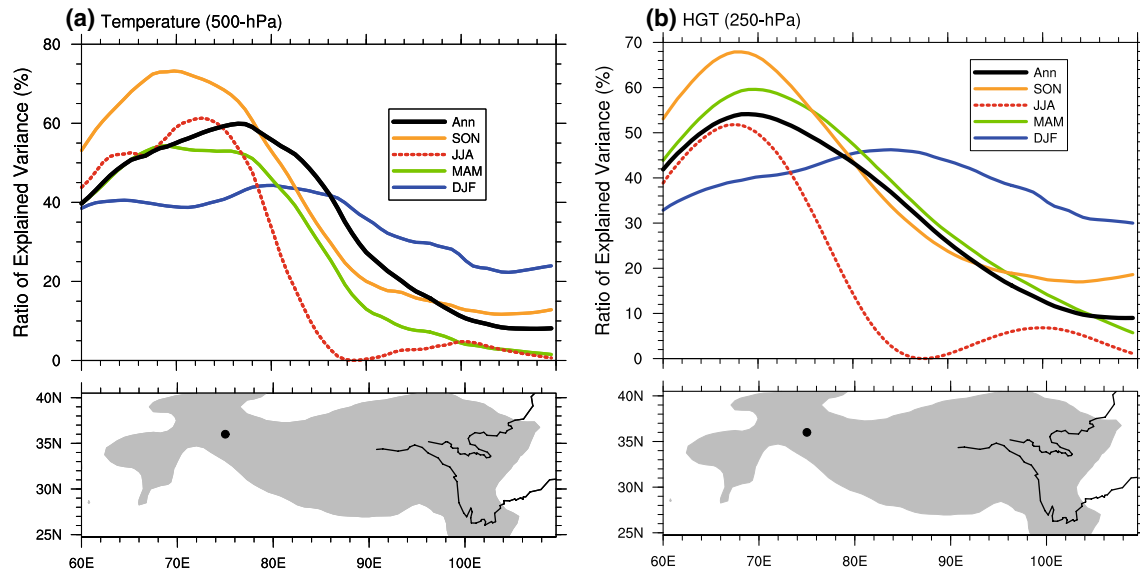


Fig. 10 The ratio (%) of the explained variance of the meridionally-averaged (24.75°N–40.5°N) **a** 500-hPa air temperature and **b** 250-hPa HGT above the Tibetan plateau by the standardized WTV intensities as a function of longitude for 1979–2016. Winter (DJF, blue solid line), spring (MAM, green solid line), summer (JJA, red dashed line), autumn (SON, orange solid line) and annual mean (bold solid line).

and winter, and causes the “West-Strong, East-Weak” pattern. In autumn, explained variance over the ETP increases to become as strong as that over the WTP (orange line in Fig. 9b), indicating that WTV variability still dominates the WTP, but that other atmospheric variability develops over the ETP and is as strong as the WTV influence over the WTP. In summer, the pattern of “West-Strong, East-Weak” (Fig. 9b) is reversed, with variance over the ETP becoming much stronger than over the WTP, although the WTV still exists over the WTP. This suggests that summer atmospheric variability over the TP as a whole is dominated by modes other than the WTV, for example, the South Asia High. However, over the annual cycle, the WTV is an important mode of variability at the near surface (500-hPa) over the whole TP. Further discussion about the weaker control of the WTV over the summertime TP near surface is included in the last section.

The dominant variability of the WTV over the WTP is also demonstrated well in the near surface (500-hPa) air temperature field and in the upper-troposphere (250-hPa) HGT. The pattern of “West-Strong, East-Weak” is also observed in the explained variance of both the near surface air temperature and the upper-tropospheric HGT by KZI variability, with explained variance high over the WTP but low over the ETP (Fig. 10a, b). Moreover, over the WTP, the maximum ratio of explained variance in both the near surface air temperature and the upper-tropospheric HGT are high, exceeding 50% in spring, summer, autumn and the annual mean

The topography of Tibetan plateau is shown in the bottom panel (24.75°N–40.5°N, 60°E–110°E), the grey shaded area denotes the topography above 1500 m. The black dot denotes the central position (36°N, 75°E) of the Karakoram focus area. Bold black curves originating in the ETP are respectively the Yangtze river and the Yellow river

(Fig. 10a, b). In addition, we also find that the explained variance in winter (blue lines in Fig. 10a, b) is more uniform over the whole TP, which coincides with the more significant WTV structure over the whole TP in the winter season (Figs. 3a, 4a). So, the WTP can explain over half of the variability in near surface air temperature and upper-troposphere HGT over the WTP in most seasons and in the annual mean.

To obtain a full view of the dominant variability of the WTV in the atmospheric circulation variability over the WTP and the neighbouring areas, we calculate the explained variance of the zonally-averaged HGT and the zonally-averaged air temperature by the KZI along the latitudinal profile across the central WTP over multiple vertical levels. Shown as Fig. 11, the maximum variance of the HGT explained by the KZI variability is located in the upper-troposphere at around 250-hPa, within the core mass column of the WTV above the WTP. The maximum ratio of explained variance of the HGT variability is over 50% in all four seasons (contours in Fig. 11a–d) and in the annual mean (contours in Fig. 11e), suggesting the WTV provides the dominant variability in upper-troposphere HGT at around 250-hPa over the WTP all year around. For the air temperature field, in contrast, the biggest explained variance of the air temperature is mainly located in both the mid-lower troposphere near to the WTP and the upper-troposphere over the WTP. Again, the maximum ratio of explained variance in air temperature by the KZI reaches above 50% in winter and above 60% in the other three seasons (colour-shading in Fig. 11a–d) and

Explained Variance over WTP

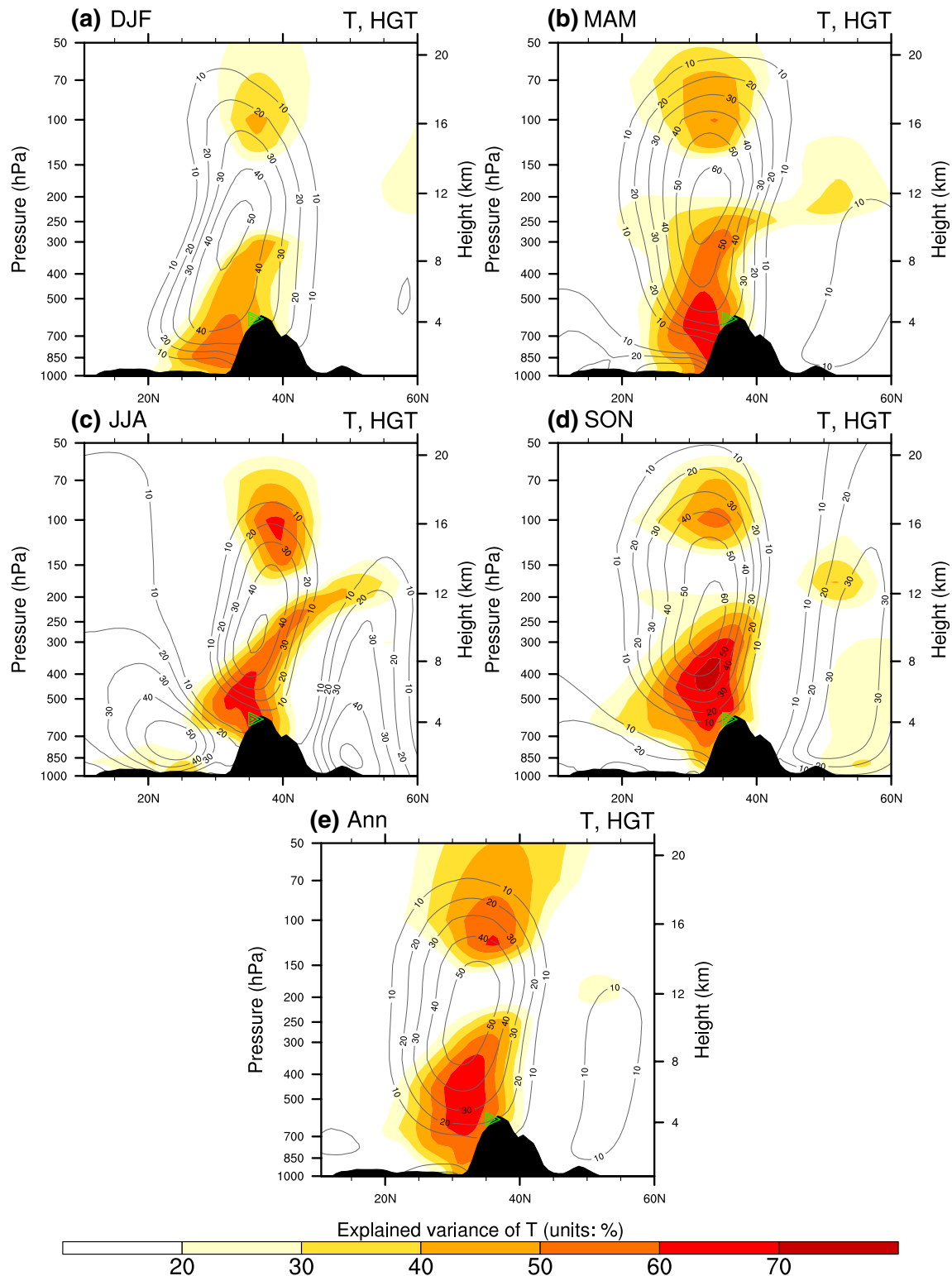


Fig. 11 The explained variance (%) of zonally-averaged geopotential height (HGT, contour) and air temperature (T, colour-shaded) along a latitudinal profile (across 70°E–80°E, central area of the WTP) by the KZI variability for 1979–2016. **a** Winter (DJF), **b** spring (MAM),

c summer (JJA), **d** autumn (SON) and **e** annual mean. The contour interval is 10. The black shaded area denotes the topography. The green triangle denotes the central Karakoram (36°N, 75°E)

in the annual mean (colour-shading in Fig. 11e). Comparing the maximum ratio of explained variance for the HGT field and air temperature in the annual mean (Fig. 11e), we find the maximum ratio of explained variance by the KZI in air temperature is greater than that for HGT. The maximum ratio of explained variance of the air temperature is located in the mid-lower troposphere, which could largely result from the fact that adiabatic processes affect air temperature more in the mid-lower troposphere than in the further aloft. Besides, the maximum ratio of explained variance of the air temperature in winter and spring (Fig. 11a, b) are located even lower than in summer and autumn (Fig. 11c, d), which coincides with the WTV having a deeper structure in winter and spring than in spring and autumn. Therefore, we

conclude that the WTV is the dominant mode of variability over the WTP, as it can explain more than half of the circulation variability at multiple levels over the WTP in most seasons and in the annual mean.

Considering potential modes of dominant atmospheric variability more generally, it should be noted that these do not necessarily explain over half of the variance in the atmospheric circulation for any given domain because the atmospheric circulation variance is usually contributed by multiple drivers simultaneously. For example, the Northern Hemisphere Annular mode (NAM) or the Arctic Oscillation (AO) is well-known (Thompson and Wallace 1998, 2000) as the dominant mode of variability in the northern extratropical atmosphere; however, it explains only around 22% of the

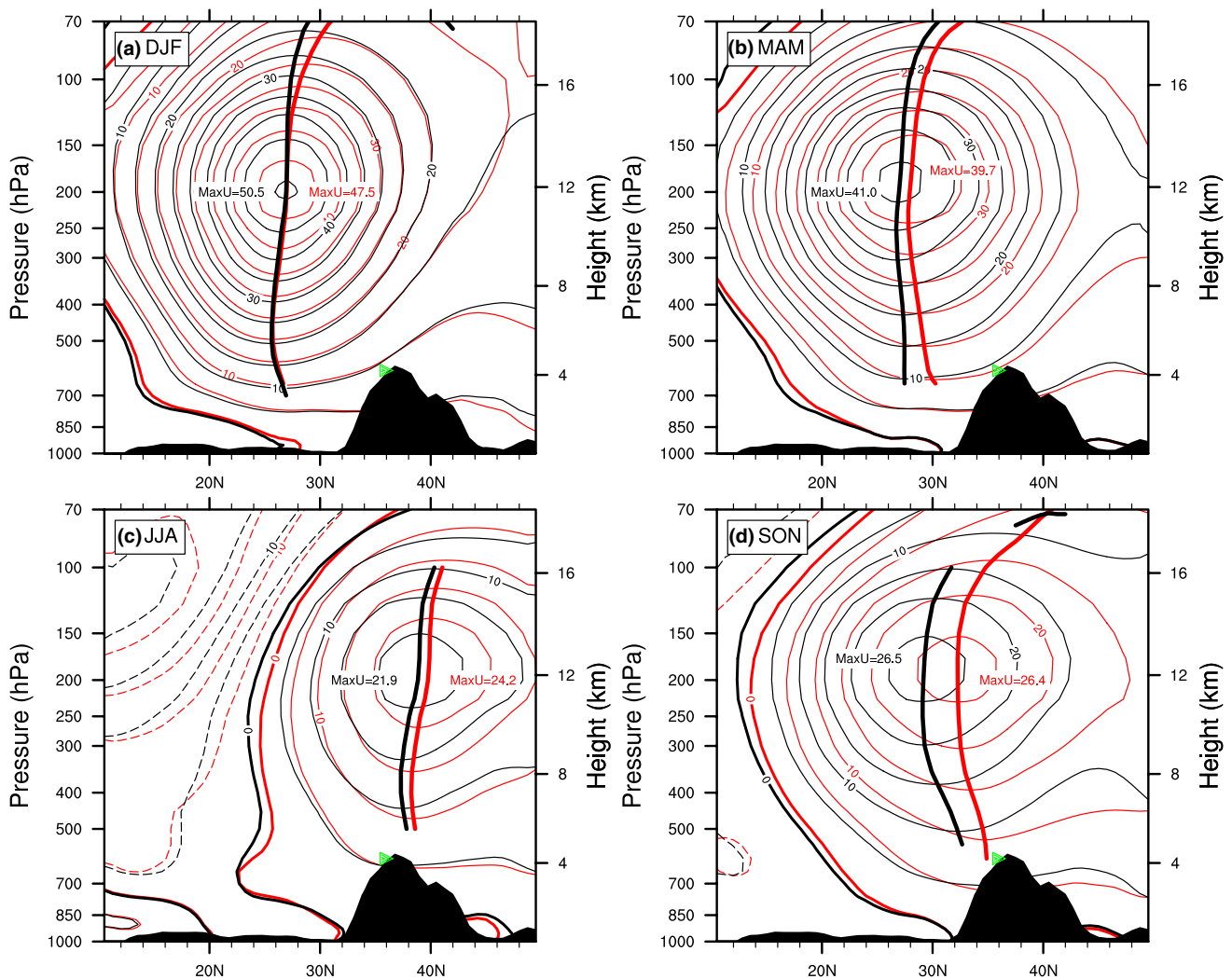


Fig. 12 The composited mean (0° – 60° E) zonal wind and axes of the subtropical westerly jet for **a** winter (DJF), **b** spring (MAM), **c** summer (JJA), and **d** autumn (SON) at multiple levels for 1979–2016. The composited zonal wind (contours, 5 m/s per interval), axes (bold vertical curves) and maximum value of the zonal wind (denoted as “MaxU”) in positive and negative KZI events are coloured in red and

black, respectively. The dashed contours denote negative values, and the bold contours denote zero. Axes where zonal wind is less than 8 m/s are masked. The black shaded area denotes the topography. The green triangle denotes the central position (36° N, 75° E) of the Karakoram focus area

total variability of extratropical circulation, i.e. the sea level pressure or the 1000-hPa HGT north of 20°N (Thompson and Wallace 1998, 2000). In contrast to the NAM/AO, the WTV can explain over 50% of the variance in atmospheric circulation across a broad vertical profile over the WTP as a single mode of variability, which is remarkable. This implies that the WTV is the single most important mode of year-to-year circulation variability over the WTP.

5 Connection of year-to-year variability of the western Tibetan vortex to the subtropical westerly jet (SWJ)

To investigate the impact of the SWJ (e.g., Holton 1992; Archer and Caldeira 2008) on the year-to-year variability of the WTV, we composited the zonal wind upstream of the TP according to the identified positive and negative KZI events, respectively (Fig. 12). A positive (negative) KZI event in a season (i.e., winter, spring, summer or autumn) is defined as the season of 1 year when the KZI is above (below) 0.5 (−0.5) times its standard deviation for that season for all years in the period 1979–2016. The location of the SWJ axis was then calculated from the composited seasonal mean zonal wind, which denotes the central locations of the subtropical jet at multiple pressure levels. The location of the SWJ axis at each level is defined as the location of the zero values of $\frac{\partial U}{\partial y}$ at each level, where U is the zonal wind and y denotes the latitude. The intensity of the SWJ is defined as the maximum value of the zonal-averaged (0°–60°E) zonal wind.

From Fig. 12, we can see that the relationship of the WTV to the intensity and location of the SWJ is highly variable from season to season. In winter, the central location of the SWJ is quite similar in both positive and negative phases of the KZI, as the axes overlap at most levels (Fig. 12a); however, the intensity of the SWJ during negative KZI events is 3 m/s higher than during positive KZI events; the largest intensity difference in all seasons. This suggests that the winter WTV is mainly impacted by the SWJ's intensity rather than its location: the weaker the SWJ, the more anti-cyclonic the KZSA and the WTV. In contrast, the WTV in autumn (Fig. 12c) is impacted more by the SWJ's location than its intensity: the more southerly-located the SWJ, the anti-cyclonic the KZSA and the WTV. This is evidenced by the largest difference in the location of the axes of the SWJ between positive and negative phase KZI events ($\sim 4^\circ$ at 200 hPa, which is about 400 km in distance in the mid-latitudes), and by the lowest difference in the intensity of the SWJ (0.1 m/s). In spring and summer, both the location and the intensity of the SWJ have an impact on the WTV. In summer, the intensity of the SWJ for positive KZI events

is greater than for negative KZI events; in all other seasons, this is reversed.

The above relationships can be attributed to the different locations of the seasonal mean SWJ relative to the TP in different seasons. Associated with seasonal changes in the solar elevation angle, the SWJ moves north and south over the TP. The SWJ is located far to the south of the TP in winter in both the negative and the positive phases of the KZI, moves closer to the TP in spring, is closest to but still south of the TP in autumn, and moves to the north of the TP in summer (Fig. 12). In winter (autumn), when the SWJ is far to the south of (near to) the TP, intensity changes of the SWJ become more (less) important for the KZSA and KZI, but location changes of the axes become less (more) important. In spring and summer, the SWJ is of medium distance from the TP, and both the intensity and location of SWJ are important. As summer is the only season in which the SWJ is located to the north of the TP, an intensification of the SWJ induces a reversed KZSA and KZI relative to other seasons (when the SWJ is located to the south of the TP). Therefore, the seasonal mean position of the SWJ relative to the TP is one important factor controlling changes in the north–south zonal wind gradients over the Karakoram, and determining seasonal relationships between the WTV and the SWJ. It has been previously reported that westerly disturbances (Cannon et al. 2015) and the North Atlantic Oscillation (Li et al. 2005, 2008) located upstream of the TP impose significant impacts on circulations surrounding the TP. Our results here provide a potential physical explanation, linking upper-level factors related to the SWJ and their impacts on the WTV. Related investigations are still ongoing but are out of scope of the current study.

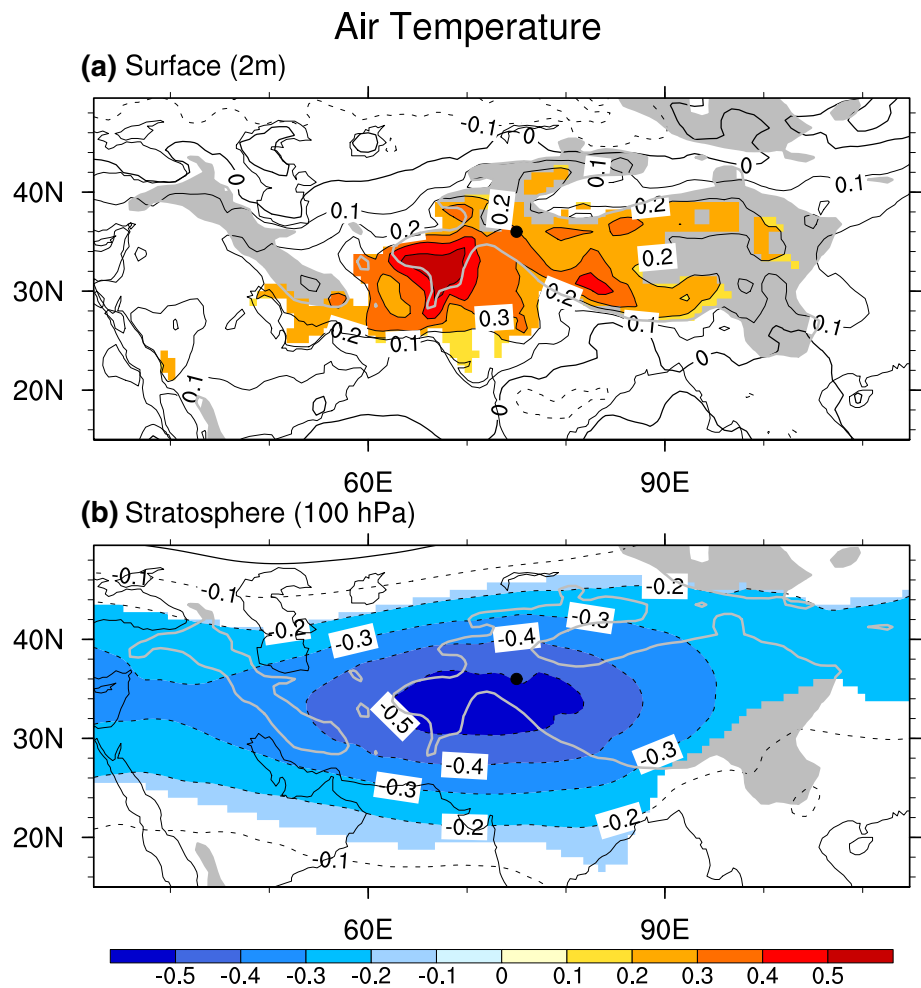
6 Temporal variation of structures associated with the western Tibetan Vortex

As the dominant vortex system over the WTP, the WTV's influence on year-to-year variability of the regional climate could be important. To verify this, we examined the varying structures of surface and stratospheric air temperature, precipitation, and ozone embedded within the year-to-year variability of the WTV.

6.1 Surface and stratospheric air temperature

The patterns in Fig. 13 show that the WTV heavily influences both surface air and stratospheric temperatures over the WTP. The top panel (Fig. 13a) shows the annual mean 2 m surface air temperature (T_{2m}) regressed upon the standardized KZI. An increase (decrease) of one standard

Fig. 13 Regression slopes of annual mean air temperature (K) onto the standardized annual time series of KZI for 1979–2016. **a** 2 m surface air temperature, **b** stratospheric air temperature at the 100 hPa level. The colour shading denotes significance above the 0.05 level after taking account of the efficient number of degrees of freedom (Zar 1984; Li et al. 2013). The black dot denotes the central position (36°N, 75°E) of the Karakoram focus area. The grey shaded area with bold-grey-outline denotes topography above 1500 m



deviation in the magnitude of the WTV results in ~ 0.4 and ~ 0.5 K warmer (cooler) T_{2m} conditions over the south-west edge and the west tail of the TP respectively, much stronger than for other regions. We also investigated the response of T_{2m} to KZI variability in all four seasons (Figures not shown), and found that the regressed T_{2m} in winter shows the broadest domain of influence on T_{2m} over the WTP, and the regressed T_{2m} in spring shows the strongest response, reaching over 1 K per standard deviation in WTV magnitude. Therefore, the impact of the WTV on surface air temperature over the WTP is considerable.

The significant influence of WTV on surface air temperature occurs because mid-lower troposphere air temperature variability above the WTP is connected significantly with the WTV through the adiabatic process (shown in Fig. 6), and the extension downward of the WTV system naturally brings its impacts to surface air temperature. Forsythe et al. (2017) also found that the WTV has significant impacts on T_{2m} over the Karakoram and surrounding area in late winter (JFM) and summer (JJA), which is consistent with the results here.

In particular, the WTV is an important driver of T_{2m} changes in the plains and low mountain areas neighbouring the WTP in winter and spring, not only the high mountain area. Since the WTV shows a deeper vertical structure in winter and spring, the response of the mid-lower troposphere air temperature extends downward to below 700 hPa in these seasons, and reaches the near surface over the plains and low mountain areas east and south of the WTP. Therefore, T_{2m} in parts of Turkmenistan, Uzbekistan, Afghanistan, Iran, Pakistan and India is significantly impacted by the WTV in winter and spring (Figures not shown). In spring especially, the magnitude of the response of T_{2m} in many of the plains and low mountain areas neighbouring the WTP can exceed 0.6 K increase (decrease) for one standard deviation of increase (decrease) in the KZI. In contrast, in summer and autumn, the WTV mainly impacts T_{2m} in the high mountain area over the WTP (Figures not shown) as the structure is shallower.

The bottom panel (Fig. 13b) shows the annual mean air temperature at 100 hPa regressed upon the standardized KZI. The significant negative response of stratospheric

Precipitation

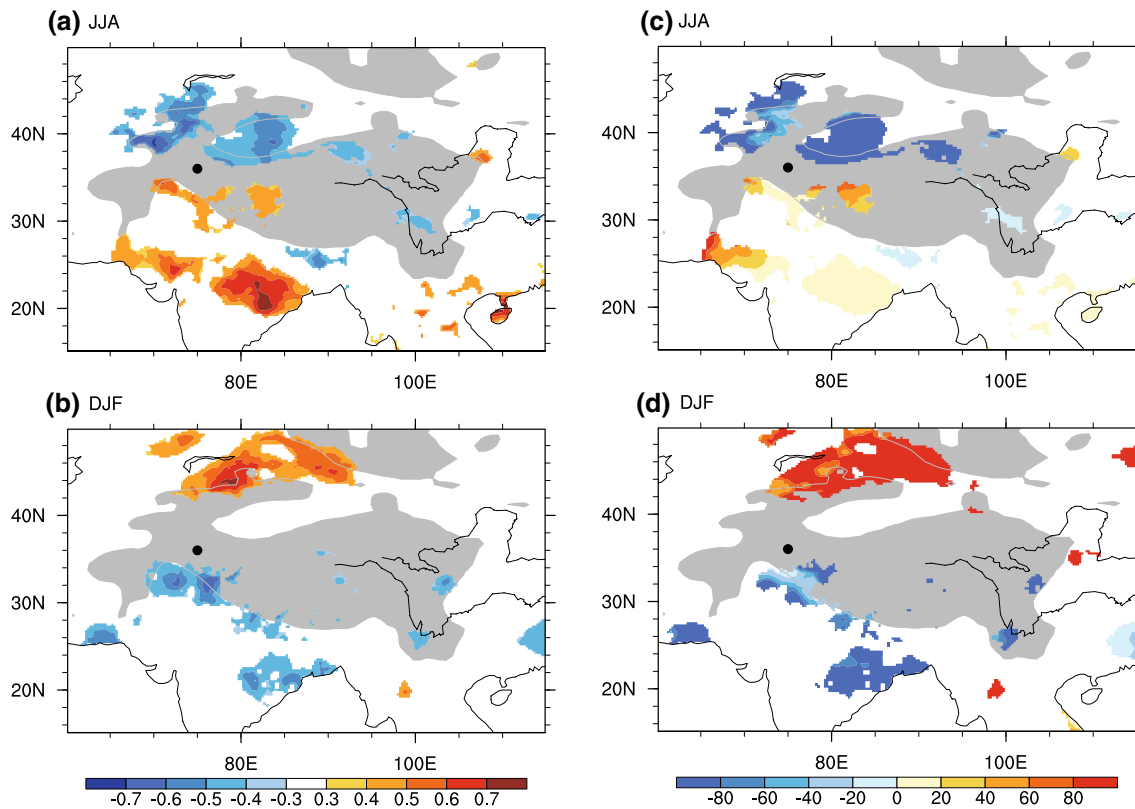


Fig. 14 Left panels are correlations between the mean precipitation and time series of KZI in **a** summer (JJA) and **b** winter (DJF), right panels are the ratio (%) of regressions of precipitation onto the standardized time series of KZI relative to seasonal mean precipitation, both for the period 1979–2007 in **c** summer (JJA) and **d** winter (DJF). The colour shading denotes significance above the 0.05 level,

temperature is of greatest magnitude over the WTP, suggesting that an anti-cyclonic WTV corresponds to cooler temperatures in the lower stratosphere, and a cyclonic WTV corresponds to warmer temperatures. Areas with significant relationships are centred on the WTP. Comparing the areas with significant relationships for all four seasons (Figures not shown), we find the signal is broadest in winter and smallest in summer, similar to the spatial patterns of HGT (Fig. 3) and temperature (Fig. 4) in the mid-lower troposphere. The negative regressions of annual mean air temperature at 100 hPa reach above 0.5 K, suggesting that one standard deviation of increase (decrease) in the KZI corresponds to more than 0.5 K cooler (warmer) stratospheric temperatures over the WTP. Specifically, the stratospheric air temperature shows its strongest connection with WTV variability in spring, when one standard deviation change in WTV corresponds to a change in stratospheric temperature of more than 1 K (Figures not shown). This implies that the whole atmospheric column of air temperature is influenced

after taking account of the efficient number of degrees of freedom (Zar 1984; Li et al. 2013). The black dot denotes the central position (36°N, 75°E) of the Karakoram focus area. The grey shaded area denotes topography above 1500 m. Bold black curves originating in the ETP are respectively the Yangtze river and the Yellow river

heavily by the WTV. The dynamical processes linking the cooler (warmer) stratospheric temperature and associated anti-cyclonic (cyclonic) WTV variability need further investigation, but are out of scope for this study.

6.2 Opposite signals in summer and winter precipitation

Precipitation variability over the Tibetan Plateau and neighbouring area has been investigated by many studies (e.g., Syed et al. 2006; Yadav 2009; Yadav et al. 2009, 2013; Dash et al. 2009; Bollasina et al. 2011; Maussion et al. 2014; Zhao et al. 2014; Saha et al. 2014). Here, we investigated precipitation variability over the region in the context of the WTV.

Interesting features identified here include opposing precipitation signals, in response to WTV variability, north and south of the TP whose signs reverse between summer and winter. In summer (Fig. 14a), the KZI is positively correlated

with precipitation over the south of the TP, including the northeast Indian subcontinent, the north and south Indus Valley, and the southwest TP, and negatively correlated with precipitation changes over the north-flank of the WTP and west Indo-Gangetic Plain. However, in winter (Fig. 14b), the above precipitation signals are generally reversed. The KZI is negatively correlated with precipitation over the south of the WTP, including the southern Iranian plateau, the northeast Indian subcontinent, the north Indus Valley, the mid-west Indo-Gangetic Plain and the southwest TP, and positively correlated over the north-flank of the WTP. This implies that an anti-cyclonic WTV corresponds to decreased precipitation over the south of the TP and increased precipitation over the north-flank of the WTP in summer and vice versa for a cyclonic WTV, which are generally opposite to conditions in winter (Fig. 14a vs Fig. 14b). Precipitation in the area near to the Karakoram (shown as the black point in Fig. 14) shows non-significant correlations with the KZI in both winter and summer. So, WTV variability is associated with the opposing north–south precipitation dipole patterns around the TP between summer and winter.

As the precipitation south of the TP is usually much greater than that north of the TP, we examined the ratio of regressed precipitation upon standardized KZI relative to the seasonal mean precipitation to produce results that are more comparable. Figure 14c, d shows that precipitation over the north-flank of the WTP in both seasons is significantly controlled by the WTV; the magnitude of precipitation variation corresponding to one standard deviation change of the WTV is large and corresponds to more than 80% of the mean precipitation in both seasons over the north-flank of the WTP. However, in the south of the WTP, corresponding precipitation changes due to WTV variability are relatively weak in summer (Fig. 14c) but stronger in winter (Fig. 14d); change in precipitation for one standard deviation change of the WTV can reach about 20% of summer mean precipitation and over 80% of winter precipitation over the northeast Indian subcontinent. In addition, the influence of the KV on precipitation over the north and south Indus Valley and the south TP is also strong in both winter and summer; change in precipitation for one standard deviation change of the WTV can reach 20–80% of mean precipitation in both seasons. Although the relative response of summer precipitation (Fig. 14c) over the lower Ganges basin is small, the absolute impact of even fractional variability of the monsoon in this area has very substantial impacts in terms of regional food security and economic activity (Immerzeel et al. 2010). Zhao et al. (2014) found that anticyclonic/cyclonic circulation similar to the WTV over the WTP influences transport of water vapour from the subtropical Indian Ocean to the Tarim Basin. Increasingly frequent cyclonic anomalies of the circulation have resulted in precipitation increases over the Tarim Basin in summer (Zhao et al. 2014). This supports

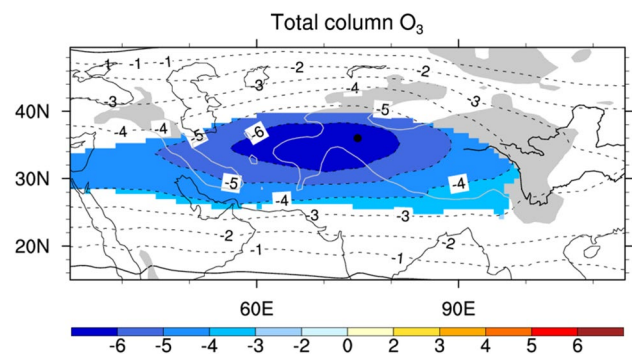


Fig. 15 Regression slopes of total column ozone (10^{-2} g m^{-2}) onto the standardized time series of the annual mean KZI for 1979–2016. The colour shading denotes significance above the 0.05 level, after taking account of the efficient number of degrees of freedom (Zar 1984; Li et al. 2013). The black dot denotes the central position (36°N , 75°E) of the Karakoram focus area. The grey shaded area denotes topography above 1500 m. Bold black curves originating in the ETP are respectively the Yangtze river and the Yellow river

the results shown here. Therefore, the WTV is one of the dominant drivers of precipitation variability over the north flank of the TP, and linked with part of the precipitation variability over the southern WTP and its neighbouring area.

The above results are based on the APHRODITE precipitation dataset. We use this dataset due to its higher quality over mountain areas compared with other gridded datasets (Yatagai et al. 2012). However, it should be noted that the extreme topography over the TP causes large uncertainties (Reggiani et al. 2016) and the quality of APHRODITE over the Karakoram area could therefore still be questionable (Immerzeel et al. 2015) due to the lower density of station observations (Figure not shown). So, denser precipitation observations over the WTP are needed to verify and extend our results.

6.3 Total column ozone

The TP is treated as the “third pole” (Yao et al. 2012) of the earth, having a thinner ozone (O_3) layer, or an “ozone valley” (e.g., Tobo et al. 2008) above it, similar to the “ozone hole” over the Arctic and Antarctic (e.g., Crutzen and Arnold 1986; Stolarski et al. 1991; Austin et al. 1992). The O_3 concentration determines the strength of solar ultraviolet rays that reach the ground (e.g., Frederick et al. 1989; Kerr and Fioletov 2008), this, in turn, influences the growth of plants (e.g., Caldwell 1981) and the skin health of human beings (e.g., Frederick 1989) in the local area. Moreover, the total column O_3 over the TP has decreased over recent decades (Zhang et al. 2014), which has caused considerable concern for the local population and great interest for scientists (e.g., Zou 1996; Zhou and Zhang 2005; Wang et al. 2006; Tian

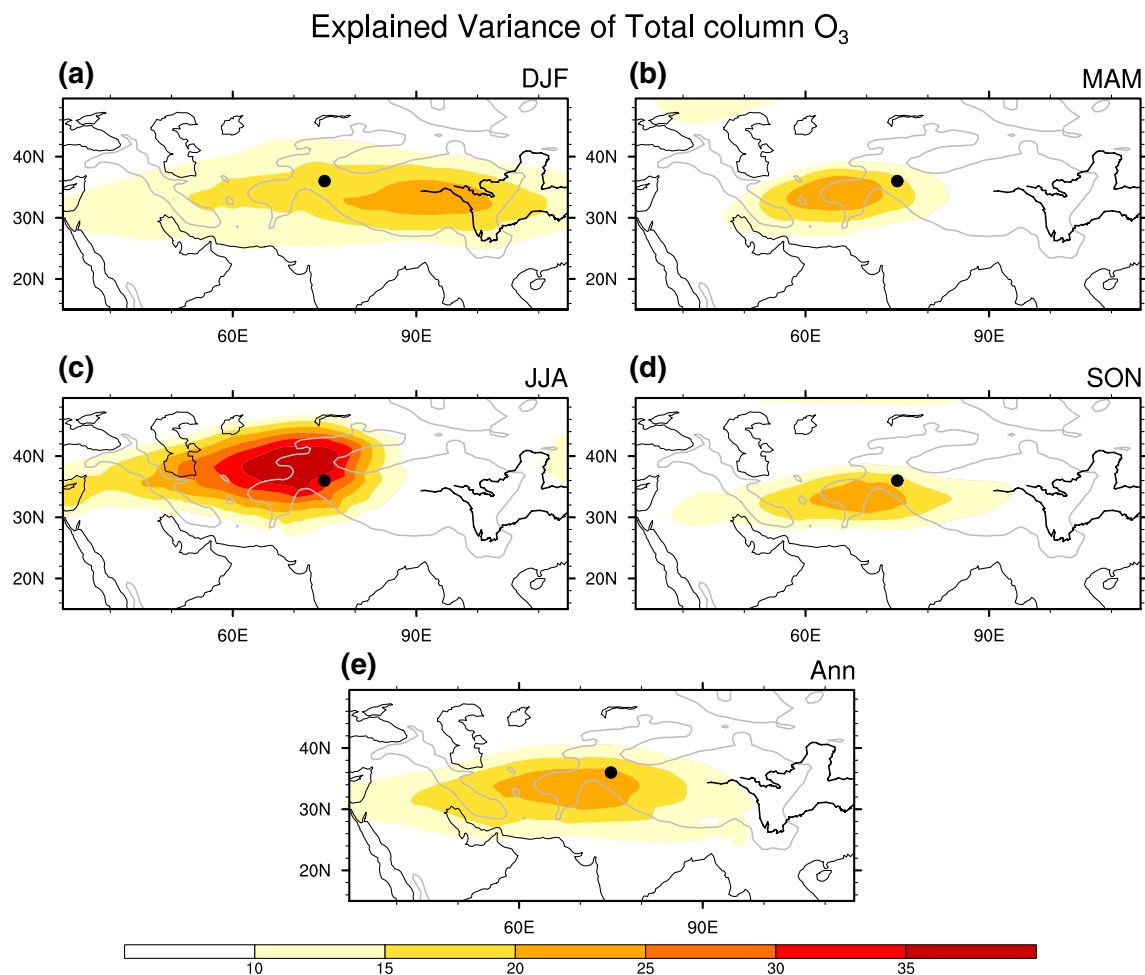


Fig. 16 The explained variance (%) of total column ozone by KZI variability for 1979–2016. **a** Winter (DJF), **b** spring (MAM), **c** summer (JJA), **d** autumn (SON) and **e** annual mean. The grey contour

denotes the topography above 1500 m. The black dot denotes the central Karakoram (36°N, 75°E). Bold black curves originating in the ETP are respectively the Yangtze river and the Yellow river

et al. 2008). Therefore, understanding O_3 changes over the TP and their link with KV variability is an important issue.

We note that the signature of the WTV in the year-to-year variability of total column ozone is significant. The regressed annual mean total column O_3 on the standardized KZI (Fig. 15) shows a negative response over the WTP. The negative response of total column O_3 to a one standard deviation increase in the KZI reaches above $6 \times 10^{-2} \text{ g m}^{-2}$. This suggests that the more anti-cyclonic (cyclonic) the WTV, the thinner (thicker) the total column ozone over the WTP. Shown as Fig. 16, for the annual mean, more than 20% of the variance of total column O_3 over the WTP responds to KZI variability. Seasonally, the KZI explains the largest portion of variance of total column O_3 over the WTP in summer (Fig. 16c), reaching above 35%. In other seasons, the KZI variability explains less of the variance of total column O_3 over the WTP, but still above 20%. In addition, in winter (Fig. 16a), the

explained variance of total column O_3 by the WTV is located over a wider area above the TP, and the maximum ratio of explained variance is located at the mid-TP, which is coincident with the larger domain of the WTV in winter. Therefore, a considerable portion of the total column O_3 variability over the WTP is explained by the WTV, and the biggest portion of the O_3 variability explained by the WTV is in the summer season.

Given that O_3 absorbs solar ultraviolet rays, an anti-cyclonic WTV could allow a larger input of ultraviolet rays to reach the surface of the WTP and surrounding areas. Because solar ultraviolet radiation is strongest in summer, and the KZI explains a large portion of the variability of the total column O_3 in summer, variability of the WTV is therefore important for the surface input of ultraviolet rays over the WTP at this time of year. The significant links between year-to-year variability in the WTV and O_3 could provide

a new way to understand and predict changes in O_3 and the “ozone valley” over the TP.

7 Discussion and conclusions

This study extends the work of Forsythe et al. (2017) by investigating in more detail features of the WTV’s seasonal and year-to-year variability, exploring its relationship with regional climate, and introducing the WTV to a wider climate community. To do this, we developed a monthly KZI based on methods from Forsythe et al. (2017) and with this studied the WTV’s basic features, its seasonality, and its signals embedded in year-to-year variability of the atmospheric circulations surrounding the WTP using ERA Interim data. We have confirmed that the WTV is active, prevails and is significantly associated with adiabatic processes in all four seasons over the WTP.

We conclude that:

1. The WTV is an important driver of atmospheric variability for the whole TP, providing the dominant mode of variability over the WTP. In the annual mean and most seasons, the WTV causes a pattern of “West-Strong, East-Weak” in the longitudinal-profile of the variance of meridional mean HGT over the whole TP. As the WTV can explain over 50% variance of the atmospheric circulation variability over the WTP on multiple levels throughout the troposphere in most seasons and in the annual mean data, this implies that it is the single most important year-to-year mode of circulation variability over the WTP.
2. The intensity and domain area of the WTV has obvious seasonality. The most active WTV emerges in winter and early spring, and a less active WTV emerges in summer and autumn. Horizontally, the WTV’s spatial domain at the near surface of the WTP is largest in winter and smallest in summer; and the cyclonic/anti-cyclonic shape of the WTV in the horizontal wind field forms a more closed circulation in spring and summer than in other seasons. Furthermore, the spatial scale of the WTV is comparable to the south Asia monsoon or the Indian monsoon system. Vertically, the WTV has a deeper structure in winter and spring than in summer and autumn.
3. The WTV is sensitive to both the intensity and location of the SWJ, but the relationships are complicated and highly dependent on the mean location of the axes of the SWJ in different seasons relative to the location of the TP. When the climatological mean SWJ is located far to the south of the TP in winter, the WTV is more sensitive to the SWJ’s intensity changes. When the SWJ is located south of, but closer to, the TP in spring, the WTV is sensitive to both the fluctuations in intensity and location of the SWJ. When the SWJ is located south of, but very near to, the TP in autumn, the intensity changes of the SWJ become less important to the WTV, and the fluctuations in the SWJ’s location become more important. When the SWJ is located to the north of the TP in summer, intensity changes of the SWJ induce a reversed change in the WTV relative to other seasons.
4. The WTV can have considerable impact on the surrounding climate. An anti-cyclonic (cyclonic) WTV causes significant warming (cooling) of surface air temperature and cooling (warming) of stratospheric air temperature over the WTP. Additionally, WTV variability is responsible for the opposing north–south precipitation dipole pattern around the TP between summer and winter. The WTV is also important for the distribution of total column ozone and the input of ultraviolet rays, especially in summer season, over the WTP, which could provide a new way to understand and predict the changes in O_3 and the “ozone valley” over the TP.

There are many questions remaining and some caveats. We show that the WTV is less active, with a smaller area of influence, over the near-surface of the WTP in summer. This could be due to the increased importance of diabatic processes associated with sensible and latent heat fluxes and radiative heating over the TP, especially over the central and eastern TP, in summer (Flohn 1960; Hahn and Manabe 1975; Wu and Liu 2000; Wu et al. 2007, 2015). These are different from the adiabatic sinking/rising processes associated with the WTV. For example, the south Asia high (SAH) is the dominant system over the TP in summer (Figure not shown), when the WTV explains the least variance (Fig. 9) over the TP. In contrast, the SAH is located relatively far from the TP in other seasons (Figure not shown), when the WTV explains more variance (Fig. 9) over the TP. Moreover, the basic thermodynamic features of the SAH and the WTV are opposite to each other. The WTV modulates the mid-lower troposphere and the surface air temperature over the WTP through adiabatic sinking/rising, which can be briefly summarized as the dynamical motion in the atmosphere inducing thermal changes, as documented in Forsythe et al. (2017) and in this study. In contrast, the SAH’s thermodynamic processes may be summarized as thermal forcing inducing dynamical motion. As documented in previous studies, in summer, the TP serves as a “thermal pump” (Wu et al. 1997, 2007) and drives the general atmospheric circulation around it: causing the South Asia Low over the near surface of the TP and the South Asia High in the upper troposphere and lower stratosphere at around 100–150 hPa (Flohn 1960; Hahn and Manabe 1975). Therefore, the SAH is basically a thermally induced system, but the WTV is not,

and the development and persistence of diabatic thermal processes over the TP could be the major reason for the weakening intensity and reduction in the domain of the WTV in summer as well as in autumn, but further investigation is needed to confirm this theory. Further complicating factors of WTV influence on near-surface temperature result from links between the WTV and cloud cover through cyclonic/anticyclonic conditions and on the influence of cloud cover on near-surface air temperature, which for the Karakoram is seasonally and diurnally asymmetrical (Forsythe et al. 2015) and depends on the relative influence of shortwave and long-wave radiative components.

Although ERA-Interim data is demonstrated by Forsythe et al. (2017) to better depict atmospheric conditions over the WTP centred on the Karakoram than other popular reanalysis datasets, there are still systematic errors due to the lack of dense station observations over the region. An example is the difference between the station-observed T_{2m} and ERA-Interim T_{2m} response to one standard deviation change of KZI over the Karakoram in summer, ~ 0.74 K (documented by Forsythe et al. 2017) and only ~ 0.5 K respectively (Figures not shown). This suggests that using ERA-Interim T_{2m} over the WTP could cause systematic underestimation of the WTV's impact on surface air temperature. Ideally, a denser station observation network is desirable for estimating the magnitude of the climate response to the variation of the WTV with higher accuracy.

Finally, as we have shown that the WTV dominates atmospheric variability in the annual mean and for most seasons over the WTP and is an important driver for the surrounding climate, the WTV is likely to be useful for understanding local weather and climate change around the WTP in the near future. Some important questions to address are: Is the WTV and its relationship to air temperature simulated well in state-of-the-art climate models? What is the decadal variability of the WTV? Does the WTV show trends related to global warming? What are the dynamical and thermal processes that drive the WTV? How is the WTV coupled with the south Asian monsoon? These are now under investigation.

Acknowledgements We thank the two anonymous reviewers who gave us constructive comments and suggestions that have improved the final version of this paper. We thank Dr. Jingjing Yu for her valuable comments and suggestions during the analysis of the results. Prof. Hayley J. Fowler is funded by the Wolfson Foundation and the Royal Society as a Royal Society Wolfson Research Merit Award (WM140025). Dr. Xiaofeng Li, Prof. Hayley J. Fowler and Dr. Stephen Blenkinsop are funded by the European Research Council Grant, INTENSE (ERC-2013-CoG-617329). Dr. Nathan Forsythe was supported during the developmental stages of KV identification work by a US National Science Foundation (NSF) Graduate Research Fellowship (ID 2006037346) award (2006–2010). Dr. David Pritchard is supported by a UK Engineering and Physical Sciences Research Council (EPSRC) doctoral training award (EP/M506382/1).

Open Access This article is distributed under the terms of the Creative Commons Attribution 4.0 International License (<http://creativecommons.org/licenses/by/4.0/>), which permits unrestricted use, distribution, and reproduction in any medium, provided you give appropriate credit to the original author(s) and the source, provide a link to the Creative Commons license, and indicate if changes were made.

References

- Archer CL, Caldeira K (2008) Historical trends in the jet streams. *Geophys Res Lett* 35(8):L08803. <https://doi.org/10.1029/2008GL033614>
- Austin J, Butchart N, Shine KP (1992) Possibility of an Arctic ozone hole in a doubled- CO_2 climate. *Nature* 360(6401):221–225. <https://doi.org/10.1038/360221a0>
- Bartlett M (1935) Some aspects of the time-correlation problem in regard to tests of significance. *J R Stat Soc* 98(3):536–543. <http://www.jstor.org/stable/2342284>
- Bolch T, Kulkarni A, Kääb A, Huggel C, Paul F, Cogley JG, Frey H, Kargel JS, Fujita K, Scheel M, Bajracharya S, Stoffel M (2012) The state and fate of Himalayan glaciers. *Science* 336(6079):310–314. <https://doi.org/10.1126/science.1215828>
- Bolch T, Pieczonka T, Mukherjee K, Shea J (2017) Brief communication: glaciers in the Hunza catchment (Karakoram) have been nearly in balance since the 1970s. *Cryosphere* 11:531–539. <https://doi.org/10.5194/tc-11-531-2017>
- Bollasina MA, Ming Y, Ramaswamy V (2011) Anthropogenic aerosols and the weakening of the South Asian summer monsoon. *Science* 334(6055):502–505. <https://doi.org/10.1126/science.1204994>
- Caldwell M (1981) Plant response to solar ultraviolet radiation. *Encycl Plant Physiol* 1:169–197
- Cannon F, Carvalho LMV, Jones C, Bookhagen B (2015) Multi-annual variations in winter westerly disturbance activity affecting the Himalaya. *Clim Dyn* 44(1–2):441–455. <https://doi.org/10.1007/s00382-014-2248-8>
- Crutzen PJ, Arnold F (1986) Nitric acid cloud formation in the cold Antarctic stratosphere: a major cause for the springtime ‘ozone hole’. *Nature* 324(6098):651–655. <https://doi.org/10.1038/324651a0>
- Dash SK, Kulkarni MA, Mohanty UC, Prasad K (2009) Changes in the characteristics of rain events in India. *Geophys Res Lett* 114:D10109. <https://doi.org/10.1029/2008JD010572>
- Dee DP, Uppala SM, Simmons AJ, Berrisford P, Poli P, Kobayashi S, Andrae U, Balmaseda MA, Balsamo G, Bauer P, Bechtold P, Beljaars ACM, Berg L, van de Bidlot J, Bormann N, Delsol C, Dragani R, Fuentes M, Geer AJ, Haimberger L, Healy SB, Hersbach H, Hólm EV, Isaksen I, Kållberg P, Köhler M, Matricardi M, McNally AP, Monge-Sanz BM, Morcrette JJ, Park BK, Peubey C, Rosnay P de, Tavolato C, Thépaut JN, Vitart F (2011) The ERA-interim reanalysis: configuration and performance of the data assimilation system. *Q J R Meteorol Soc* 137(656):553–597. <https://doi.org/10.1002/qj.828>
- Flohn H (1960) Recent investigation on the mechanism of the ‘summer monsoon’ of southern and eastern Asia. *Proc. symp. monsoon of the world*, Hind Union Press, pp 75–88
- Forsythe N, Hardy AJ, Fowler HJ, Blenkinsop S, Kilsby CG, Archer DR, Hashmi MZ (2015) A detailed cloud fraction climatology of the upper Indus basin and its implications for near-surface air temperature. *J Clim* 28(9):3537–3556. <https://doi.org/10.1175/JCLI-D-14-00505.1>
- Forsythe N, Fowler HJ, Li X-F, Blenkinsop S, Pritchard D (2017) Karakoram temperature and glacial melt driven by regional

- atmospheric circulation variability. *Nat Clim Change*. <https://doi.org/10.1038/nclimate3361>
- Frederick U (1989) Potential effects of altered solar ultraviolet radiation on human skin cancer. *Photochem Photobiol* 50(4):507–513. <https://doi.org/10.1111/j.1751-1097.1989.tb05556.x>
- Frederick JE, Snell HE, Haywood EK (1989) Solar ultraviolet radiation at the earth's surface. *Photochem Photobiol* 50(4):443–450. <https://doi.org/10.1111/j.1751-1097.1989.tb05548.x>
- Gardelle J, Berthier E, Arnaud Y (2012) Slight mass gain of Karakoram glaciers in the early twenty-first century. *Nat Geosci* 5(5):322–325. <https://doi.org/10.1038/ngeo1450>
- Hahn DG, Manabe S (1975) The role of mountains in the south Asian monsoon circulation. *J Atmos Sci* 32:1515–1541. [https://doi.org/10.1175/1520-0469\(1975\)032<1515:TROMIT>2.0.CO;2](https://doi.org/10.1175/1520-0469(1975)032<1515:TROMIT>2.0.CO;2)
- Hewitt K (2005) The Karakoram anomaly? Glacier expansion and the 'Elevation effect' Karakoram Himalaya. *Mt Res Dev* 25(4):332–340. [https://doi.org/10.1659/0276-4741\(2005\)025\[0332:TKAGEA\]2.0.CO;2](https://doi.org/10.1659/0276-4741(2005)025[0332:TKAGEA]2.0.CO;2)
- Holton JR (1992) An introduction to dynamic meteorology. Elsevier, New York
- Holton JR (2004) An introduction to dynamic meteorology, vol 88, 4th edn. Elsevier Academic Press, Amsterdam, p 535
- Immerzeel WW, van Beek LP, Bierkens MF (2010) Climate change will affect the Asian water towers. *Science* 328(5984):1382–1385. <https://doi.org/10.1126/science.1183188>
- Immerzeel WW, Wanders N, Lutz AF, Shea JM, Bierkens MFP (2015) Reconciling high-altitude precipitation in the upper Indus basin with glacier mass balances and runoff. *Hydrol Earth Syst Sci* 19(11):4673–4687. <https://doi.org/10.5194/hess-19-4673-2015>
- Jacob T, Wahr J, Pfeffer TW, Swenson S (2012) Recent contributions of glaciers and ice caps to sea level rise. *Nature* 482:514–518. <https://doi.org/10.1038/nature10847>
- Kääb A, Berthier E, Nuth C, Gardelle J, Arnaud Y (2012) Contrasting patterns of early twenty-first-century glacier mass change in the Himalayas. *Nature* 488(7412):495–498. <https://doi.org/10.1038/nature11324>
- Kerr JB, Fioletov VE (2008) Surface ultraviolet radiation. *Atmos Ocean* 46(1):159–184. <https://doi.org/10.3137/ao.460108>
- Li J, Yu R, Zhou T, Wang B (2005) Why is there an early spring cooling shift downstream of the Tibetan plateau? *J Clim* 18(22):4660–4668
- Li J, Yu R, Zhou T (2008) Teleconnection between NAO and climate downstream of the Tibetan plateau. *J Clim* 21(18):4680–4690
- Li X-F, Yu J, Li Y (2013) Recent summer precipitation increase and surface cooling over Northern Australia since the late 1970s: a response to warming in the tropical Western Pacific. *J Clim* 26:7221–7239. <https://doi.org/10.1175/JCLI-D-12-00786.1>
- Maussion F, Scherer D, Mölg T, Collier E, Curio J, Finkelnburg R (2014) Precipitation seasonality and variability over the Tibetan plateau as resolved by the high Asia reanalysis. *J Clim* 27(5):1910–1927. <https://doi.org/10.1175/JCLI-D-13-00282.1>
- Pratap B, Dobhal DP, Bhambr R, Mehta M, Tewari VC (2016) Four decades of glacier mass balance observations in the Indian Himalaya. *Reg Environ Change* 16(3):643–658. <https://doi.org/10.1007/s10113-015-0791-4>
- Reggiani P, Coccia G, Mukhopadhyay B (2016) Predictive uncertainty estimation on a precipitation and temperature reanalysis ensemble for Shigar basin, Central Karakoram. *Water* 8(6):263. <https://doi.org/10.3390/w8060263>
- Saha A, Ghosh S, Sahana AS, Rao EP (2014) Failure of CMIP5 climate models in simulating post-1950 decreasing trend of Indian monsoon. *Geophys Res Lett* 41(20):7323–7330. <https://doi.org/10.1002/2014GL061573>
- Stolarski RS, Bloomfield P, McPeters RD, Herman JR (1991) Total ozone trends deduced from Nimbus 7 TOMS data. *Geophys Res Lett* 18(6):1015–1018. <https://doi.org/10.1029/91GL01302>
- Syed FS, Giorgi F, Pal JS, King MP (2006) Effect of remote forcings on the winter precipitation of central southwest Asia part 1: observations. *Theoret Appl Climatol* 86(1–4):147–160. <https://doi.org/10.1007/s00704-005-0217-1>
- Thompson DWJ, Wallace JM (1998) The Arctic oscillation signature in the wintertime geopotential height and temperature fields. *Geophys Res Lett* 25(9):1297–1300. <https://doi.org/10.1029/98GL00950>
- Thompson DWJ, Wallace JM (2000) Annular modes in the extratropical circulation. Part I: month-to-month variability. *J Clim* 13(5):1000–1016. [https://doi.org/10.1175/1520-0442\(2000\)013<1000:AMITEC>2.0.CO;2](https://doi.org/10.1175/1520-0442(2000)013<1000:AMITEC>2.0.CO;2)
- Tian W, Chipperfield M, Huang Q (2008) Effects of the Tibetan plateau on total column ozone distribution. *Tellus* 60(4):622–635. <https://doi.org/10.1111/j.1600-0889.2008.00338.x>
- Tobo Y, Iwasaka Y, Zhang D, Shi G, Kim Y-S, Tamura K, Ohashi T (2008) Summertime “ozone valley” over the Tibetan Plateau derived from ozonesondes and EP/TOMS data. *Geophys Res Lett* 35(16):L16801. <https://doi.org/10.1029/2008gl034341>
- Wang T, Wong H, Tang J, Ding A, Wu W, Zhang X (2006) On the origin of surface ozone and reactive nitrogen observed at a remote mountain site in the northeastern Qinghai-Tibetan Plateau, western China. *J Geogr Sci* 111(D8):D08303
- Watanabe T, Yamazaki K (2012) Influence of the anticyclonic anomaly in the subtropical jet over the Western Tibetan plateau on the intraseasonal variability of the summer Asian monsoon in early summer. *J Clim* 25(4):1291–1303. <https://doi.org/10.1175/JCLI-D-11-00036.1>
- Wu G, Liu Y (2000) Thermal adaptation, overshooting, dispersion, and subtropical anticyclone part I: thermal adaptation and overshooting. *Sci Atmos Sin* 24(4):433–446
- Wu G, Zhang X, Liu H, Yu Y, Jin X, Guo Y, Sun S, Li W, Wang B, Shi G (1997) Global ocean-atmosphere-land system model of LASG (GOALS/LASG) and its performance in simulation study. *Q J Appl Meteorol* 8:15–28
- Wu G, Liu Y, Zhang Q, Duan A, Wang T, Wan R, Liu X, Li W, Wang Z, Liang X (2007) The influence of mechanical and thermal forcing by the Tibetan plateau on Asian climate. *J Hydrometeorol* 8:770–789. <https://doi.org/10.1175/JHM609.1>
- Wu G, Duan A, Liu Y, Mao J, Ren R, Bao Q, He B, Liu B, Hu W (2015) Tibetan Plateau climate dynamics: recent research progress and outlook. *Natl Sci Rev* 2(1):100–116. <https://doi.org/10.1093/nsr/nwu045>
- Yadav RK (2009) Changes in the large-scale features associated with the Indian summer monsoon in the recent decades. *Int J Climatol* 29(1):117–133. <https://doi.org/10.1002/joc.1698>
- Yadav RK, Kumar KR, Rajeevan M (2009) Increasing influence of ENSO and decreasing influence of AO/NAO in the recent decades over northwest India winter precipitation. *J Geophys Res* 114:D12112. <https://doi.org/10.1029/2008JD011318>
- Yadav RK, Ramu DA, Dimri AP (2013) On the relationship between ENSO patterns and winter precipitation over North and Central India. *Global Planet Change* 107:50–58. <https://doi.org/10.1016/j.gloplacha.2013.04.006>
- Yao T, Thompson LG, Mosbrugger V, Zhang F, Ma Y, Luo T, Xu B, Yang X, Joswiak DR, Wang W (2012) Third pole environment (TPE). *Environ Dev* 3:52–64. <https://doi.org/10.1016/j.envdev.2012.04.002>
- Yatagai A, Kamiguchi K, Arakawa O, Hamada A, Yasutomi N, Kitch A (2012) APHRODITE: constructing a long-term daily gridded precipitation dataset for Asia based on a dense network of rain gauges. *Bull Am Meteorol Soc* 93:1401–1415. <https://doi.org/10.1175/BAMS-D-11-00122.1>

- Zar JH (1984) Biostatistical analysis. Prentice Hall, Upper Saddle River, p 718
- Zhang J, Tian W, Xie F, Tian H, Luo J, Zhang J, Liu W, Dhomse S (2014) Climate warming and decreasing total column ozone over the Tibetan plateau during winter and spring. *Tellus B Chem Phys Meteorol* 66(1):23415. <https://doi.org/10.3402/tellusb.v66.23415>
- Zhao Y, Huang A, Zhou Y, Huang D, Yang Q, Ma Y, Li M, Wei G (2014) Impact of the middle and upper tropospheric cooling over Central Asia on the summer precipitation in the Tarim basin, China. *J Clim* 27(12):4721–4732. <https://doi.org/10.1175/JCLI-D-13-00456.1>
- Zhou S, Zhang R (2005) Decadal variations of temperature and geopotential height over the Tibetan plateau and their relations with Tibet ozone depletion. *Geophys Res Lett* 32(18):L18705. <https://doi.org/10.1029/2005GL023496>
- Zhou Y, Li Z, Li JI (2017) Slight glacier mass loss in the Karakoram region during the 1970s to 2000 revealed by KH-9 images and SRTM DEM. *J Glaciol* 63(238):331–342. <https://doi.org/10.1017/jog.2016.142>
- Zou H (1996) Seasonal variation and trends of TOMS ozone over Tibet. *Geophys Res Lett* 23(9):1029–1032. <https://doi.org/10.1029/96GL00767>